

Review

Properties and Applications of Metal Phosphates and Pyrophosphates as Proton Conductors

Rosario M. P. Colodrero , Pascual Olivera-Pastor, Aurelio Cabeza  and Montse Bazaga-García * 

Departamento de Química Inorgánica, Cristalografía y Mineralogía, Facultad de Ciencias, Universidad de Málaga, Campus Teatinos s/n, 29071 Málaga, Spain; colodrero@uma.es (R.M.P.C.); poliverap@uma.es (P.O.-P.); aurelio@uma.es (A.C.)

* Correspondence: m.bazaga@uma.es

Abstract: We review the progress in metal phosphate structural chemistry focused on proton conductivity properties and applications. Attention is paid to structure–property relationships, which ultimately determine the potential use of metal phosphates and derivatives in devices relying on proton conduction. The origin of their conducting properties, including both intrinsic and extrinsic conductivity, is rationalized in terms of distinctive structural features and the presence of specific proton carriers or the factors involved in the formation of extended hydrogen-bond networks. To make the exposition of this large class of proton conductor materials more comprehensive, we group/combine metal phosphates by their metal oxidation state, starting with metal (IV) phosphates and pyrophosphates, considering historical rationales and taking into account the accumulated body of knowledge of these compounds. We highlight the main characteristics of super protonic CsH_2PO_4 , its applicability, as well as the affordance of its composite derivatives. We finish by discussing relevant structure–conducting property correlations for divalent and trivalent metal phosphates. Overall, emphasis is placed on materials exhibiting outstanding properties for applications as electrolyte components or single electrolytes in Polymer Electrolyte Membrane Fuel Cells and Intermediate Temperature Fuel Cells.

Keywords: metal phosphate; proton conductivity; super protonic conductors; fuel cells; H-bond network; proton carriers



Citation: Colodrero, R.M.P.; Olivera-Pastor, P.; Cabeza, A.; Bazaga-García, M. Properties and Applications of Metal Phosphates and Pyrophosphates as Proton Conductors. *Materials* **2022**, *15*, 1292. <https://doi.org/10.3390/ma15041292>

Academic Editor:
Arunas Ramanavicius

Received: 29 December 2021

Accepted: 3 February 2022

Published: 9 February 2022

Publisher's Note: MDPI stays neutral with regard to jurisdictional claims in published maps and institutional affiliations.



Copyright: © 2022 by the authors. Licensee MDPI, Basel, Switzerland. This article is an open access article distributed under the terms and conditions of the Creative Commons Attribution (CC BY) license (<https://creativecommons.org/licenses/by/4.0/>).

1. Introduction

Metal phosphates (MPs) comprise an ample class of structurally versatile acidic solids, with outstanding performances in a wide variety of applications, such as catalysts [1–3], fuel cells [4–6], batteries [7], biomedical [8], etc. Depending on the metal/phosphate combinations and the synthetic methodologies, MP solids can be prepared in a vast diversity of crystalline forms, from 3D open-frameworks, through layered networks, to 1D polymeric structures.

The advantages of these solids are, among others, their low cost and easy preparation, hydrophilic and thermal stability and structural designability to a certain extent. Additionally, their structures are amenable to post-synthesis modifications, including the incorporation of ionic or neutral species that significantly affect their functionality and other important properties, such as the formation of hydrogen bonding networks or insertion of proton carriers.

While tetravalent and monovalent metal phosphates are usually prepared by conventional synthetic routes, the synthesis of many divalent and trivalent metal phosphates requires the presence of organic molecules/ions as structure-directing agents, some of which also act as charge-compensating ions [9]. In any case, the metal phosphates contain acidic phosphate groups (H_2PO_4^- and HPO_4^{2-}) or they can result from specific post-synthesis acid–base reactions, thus, allowing a mostly intrinsic proton conduction.

Additionally, an extrinsic proton conduction, associated with surface proton transport, can also result from specific chemical modification and/or induced morphological changes, e.g., with formation of nanoplatelets or nanorods particles [10,11]. Water molecules act both in the formation H-bonding networks inside the framework and as proton carriers. Moreover, other guest species, including organic moieties, can be inserted in their structure following different strategies, such as intercalation [12–14], template [15,16], and post-synthesis adsorption [17–19].

Accordingly, proton transport in MPs results from the interplay between water/guest molecules and the hydrophilic network/framework walls in specific ways. Thus, in metal phosphates, such as CsH_2PO_4 [20] or $\text{CaHPO}_4 \cdot 2\text{H}_2\text{O}$ [21] the proton-transfer mechanism involves not only the jump of H^+ but also the free rotation of the phosphate groups. In other cases, such as for KH_2PO_4 the proton-transfer mechanism behavior is by defects [22].

A more complex proton-transfer process arise from the so called “quasi-liquid” state, such as described for $\text{H}_3\text{OUO}_2\text{PO}_4 \cdot 3\text{H}_2\text{O}$ [23,24], or it may stem from various mobile species moving on the surface, each one using different paths at different rates, e.g., in $\text{Ce}(\text{HPO}_4)_2 \cdot n\text{H}_2\text{O}$ [25,26]. The proton transport in the quasi-liquid state is often characterized by a “proton jump” or the Grotthuss mechanism, with low activation energy (E_a) [21].

Determining proton conduction mechanisms is key to designing proton conductor materials (Figure 1). Thus, if a vehicle-type mechanism is needed, proton-containing counter ions, such as hydronium ions, NH_4^+ , protonated amine groups, and protonated organic molecules in general, should be incorporated into the structure. Additionally, the immobilization of specific functional groups and the corresponding counter ions onto the framework could be required.

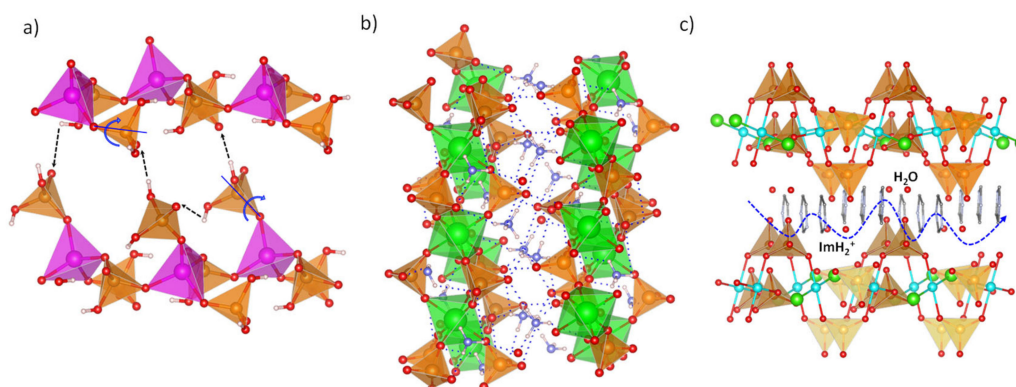


Figure 1. Examples of proton transport in phosphate-containing materials: (a) structural reorientation-mediated proton transfer. Zn (magenta), P (orange), O (red) and H (pale pink). (b) hopping through H-bond networks, and (c) carrier-mediated proton conduction. Zn (magenta), Zr (green), Cu (cyan), Cl (light green), P (orange), O (red), N (blue) and H (pale pink) atoms.

On the other hand, solids exhibiting proton transport by a Grotthuss-type mechanism basically consist of continuous H-bond networks that favour H^+ conduction with low activation energy (E_a). A main drawback for the latter materials is that, above certain temperatures, breaking of the H-bond networks can result, accompanied by the release of water molecules, which makes the construction of permanent H-bonding networks with hydrophilic channels or exploring new alternative conductive media necessary [27].

A research area of paramount interest is that relative to fuel-cell (FC) development regarding energy efficiency, environmental issues, and the gradual depletion of conventional fuel reserves [28,29]. The operating temperature regime of these electrochemical devices is determined by the electrolyte. Among the many types of solid electrolytes that have been developed over the past several decades [30], perfluorinated sulfonic acid (PFSA) ionomers,

such as Nafion[®] and Aquivion[®], are the most widely used in PEMFCs and DMFCs as polymer electrolyte membranes (PEM) for operating temperatures <120 °C.

This is due to superior conductive properties, ranging from $9 \times 10^{-3} \text{ S}\cdot\text{cm}^{-1}$ to $1.2 \times 10^{-1} \text{ S}\cdot\text{cm}^{-1}$, and chemical and mechanical stability [31,32]. This PEM acts as a separator for the reactants and, at the same time, provides pathways for proton transport [33,34]. However, Nafion[®] also shows some important drawbacks, such as methanol permeability, high costs, and complex steps of preparation, working below 100 °C to maintain the hydration of the membrane and other issues related to catalyst efficiency. All this makes necessary the development of new membrane materials [35,36].

Intermediate Temperature fuel cells (ITFCs), which operate between 120 and 300 °C, circumvent some of these problems, achieve less catalyst poisoning and better handling of the hydration conditions, and enable the use of non-precious or low-loading precious metal catalysts [37–39]. Nevertheless, for the case of methanol HT-PEMFCs, which must operate above 250 °C and with high pressure, possible degradation of the electrolytes should be a subject of study [40]. Some MP-based electrolytes gather proton conductivity properties to be used as single electrolytes or main components for ITFC applications. Examples are superprotonic CsH_2PO_4 [41] and $\text{M(IV)P}_2\text{O}_7$ -based electrolytes [42].

This review summarizes the state of the art on proton conductive metal phosphates with special attention to the last two decades of developments. A review of publication trends, from the CAS SciFinderⁿ database, is given in Figure 2, which confirms the increasing interest in this topic during this period. In this article, our focus is placed on updating recent advances in proton conductors based on tetravalent metal phosphates/pyrophosphates and superprotonic Cs_2HPO_4 . In addition, the design and development of new proton carrier systems relying on divalent and trivalent metal phosphates are also revised.

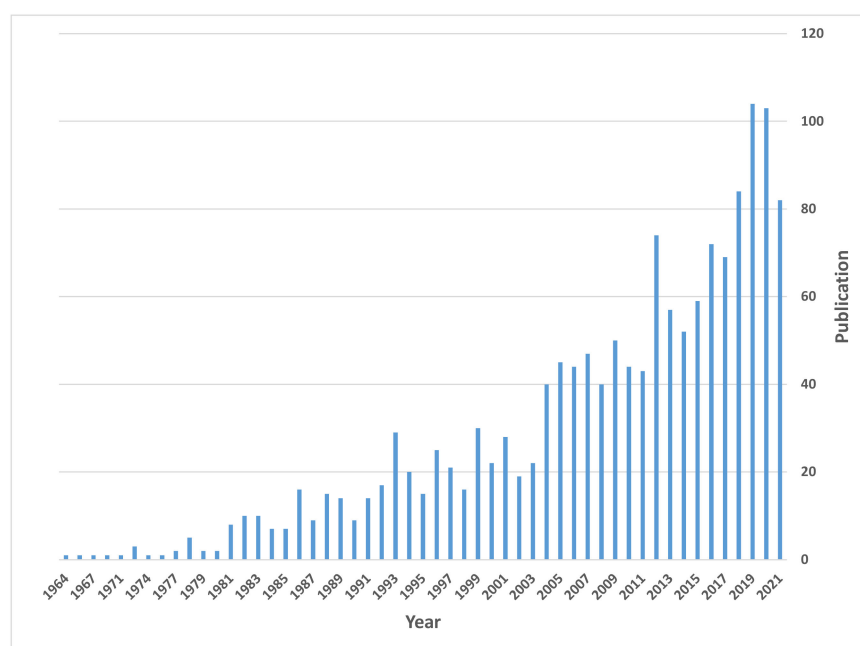


Figure 2. Publications on metal phosphates and pyrophosphate proton conductors over time.

The potential applications of these materials as proton conductor electrolytes for PEMFCs and ITFCs are also discussed. Other high temperature (above 300 °C) conductive metal phosphates, such as rare earth phosphates and metal polyphosphates, ionic conductors (e.g., NASICON), and electrode materials are out the scope of this revision. The review is not intended to be exhaustive, and therefore certain specific reports and/or applications may not be covered.

2. Tetravalent Metal Phosphates and Pyrophosphates

2.1. Zirconium Phosphates

The prototype of layered metal(IV) phosphates is zirconium hydrogen phosphate, which presents mainly three topologies, known as the forms α : $\text{Zr}(\text{HPO}_4)_2 \cdot \text{H}_2\text{O}$ (α -ZrP), γ : $\text{Zr}(\text{PO}_4)(\text{O}_2\text{P}(\text{OH})_2) 2\text{H}_2\text{O}$ (γ -ZrP), and λ : $(\text{Zr}(\text{PO}_4)\text{XY})$, X = halides, OH^- , HSO_4^- , and Y = DMTHUS, H_2O , etc.) (λ -ZrP). α -ZrP is the most thermal and hydrolytically stable phase and, thus, the most studied compound following the pioneering works by Giulio Alberti and Abraham Clearfield groups [43–45].

In the structure of α -ZrP, planar Zr atoms are coordinated by the three oxygen atoms of HO-PO_3^- groups, while the P-OH bond points toward the interlayer space giving rise to small cavities, where the lattice water is located. Although this water forms hydrogen bonds with P-OH groups, an extended interlayer hydrogen bond network is absent in this structure [44]. On the other hand, the structure of γ -ZrP consists of a biplanar Zr atomic system connected through bridge PO_4^{3-} groups, while the externally located H_2PO_4^- groups complete the octahedral coordination of the Zr atoms.

Due to the higher stability of the α form, proton conductivity studies have been conducted mainly with this phase. Typical values of 10^{-6} – 10^{-4} $\text{S}\cdot\text{cm}^{-1}$ have been determined at RT and 90% RH with activation energy (E_a) ranging between 0.26 (90% RH) and 0.52 eV (5% RH). This conductivity originates from surface transport and is dominated by surface hydration since the long distance between adjacent P-OH groups hinders proton diffusion along the internal layer surface [46].

According to theoretical estimations [47], the interactions between POH and water molecules on the zirconium phosphate surface are relatively large and generate strong local hydrogen-bond networks. The high density of acid groups should produce continuous short O-O distances and generate proton-transfer paths with low activation energy, even under high-temperature and low-humidity conditions.

Studies on microcrystalline α -ZrP revealed that both the morphology and the electric field orientation are important aspects to consider. Thus, pellicular samples of α -ZrP, prepared by intercalation-deintercalation of n-propylamine [48], exhibited a proton conductivity of 10^{-4} $\text{S}\cdot\text{cm}^{-1}$ at 300 °C when it was measured with the electric field parallel to the pellicles. This conductivity was found to be approximately two orders of magnitude higher than that measured on applying the electric field perpendicular to the pellicles [49].

Several other strategies to increase the proton conductivity of α -ZrP have been developed (Table 1). One of the first approaches was the formation of polyhydrated n-propylamine-intercalated compounds ($\text{ZrP}\cdot x\text{PrNH}_2\cdot n\text{H}_2\text{O}$). For a composition with $x = 0.8$ and $n = 5$, a proton conductivity of 1.2×10^{-3} $\text{S}\cdot\text{cm}^{-1}$ at 20 °C and 90% RH was determined [50]. Another more sophisticated way of enhancing the proton conductivity of zirconium phosphate was the preparation of mesoporous zirconium phosphate/pyrophosphate, $\text{Zr}(\text{P}_2\text{O}_7)_{0.81}(\text{O}_3\text{POH})_{0.38}$.

This material, obtained from the thermal decomposition of zirconium phosphite benzenediphosphonate, displayed a high specific surface area ($215 \text{ m}^2/\text{g}$) with an enhanced proton conductivity of 1.3×10^{-3} $\text{S}\cdot\text{cm}^{-1}$ at 20 °C and 90% RH [51]. One of the most successful ways of obtaining zirconium phosphate derivatives with outstanding proton conductivity properties consisted in preparing mixed zirconium phosphate/phosphonates, an example being $[\text{Zr}(\text{O}_3\text{POH})_{2-x}(\text{O}_3\text{PC}_6\text{H}_4\text{SO}_3\text{H})_x]$, whose proton conductivity was found to increase with x , up to a value of 0.07 $\text{S}\cdot\text{cm}^{-1}$ ($x = 1.35$ at 100 °C and 90% RH) [52].

The great versatility of zirconium phosphate preparation under numerous experimental conditions, has been exploited to synthesize various novel derivatives, which displayed remarkable proton conductivity properties. Two examples are layered $(\text{NH}_4)_2[\text{ZrF}_2(\text{HPO}_4)_2]$ [53] and the 3D open framework zirconium phosphate $(\text{NH}_4)_5[\text{Zr}_3(\text{OH})_3\text{F}_6(\text{PO}_4)_2(\text{HPO}_4)]$ [54]. In both structures, the participation of NH_4^+ ions in the formation of extended hydrogen-bond networks (Figure 3) resulted in proton conductivities of 1.45×10^{-2} $\text{S}\cdot\text{cm}^{-1}$ (at 90 °C and 95% RH) and 4.41×10^{-2} $\text{S}\cdot\text{cm}^{-1}$ (at 60 °C and 98% RH), respectively. From

the E_a values found, 0.19 and 0.33 eV, respectively, a Grotthuss-type proton-transfer mechanism was inferred for these materials (Table 1).

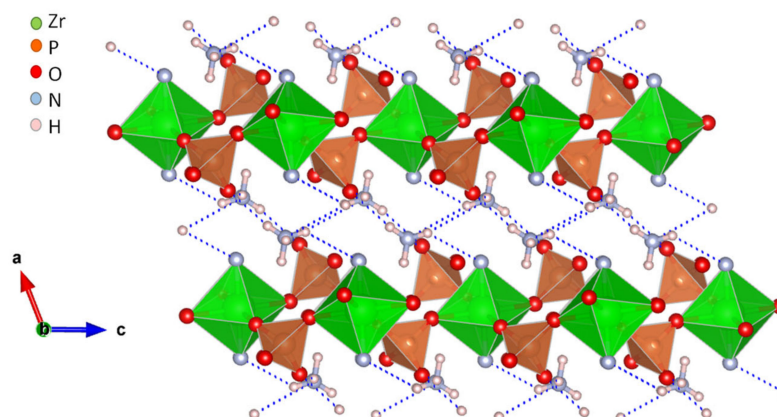


Figure 3. Layered structure of compound $(\text{NH}_4)_2[\text{ZrF}_2(\text{HPO}_4)_2]$ and possible proton-transfer pathways (adapted from [53]).

A one-dimensional zirconium phosphate, $(\text{NH}_4)_3\text{Zr}(\text{H}_{2/3}\text{PO}_4)_3$, consisting of anionic $[\text{Zr}(\text{H}_{2/3}\text{PO}_4)_3]^{3-}$ chains bonded to charge-compensating NH_4^+ ions was reported [55]. In this structure, the phosphates groups are disorderly protonated, while NH_4^+ ions occupy ordered positions in between adjacent chains (Figure 4). This arrangement generates H-bonding infinite chains of acid–base pairs ($\text{N}-\text{H}\cdots\text{O}-\text{P}$) that lead to a high proton conductivity in anhydrous state of $1.45 \times 10^{-3} \text{ S}\cdot\text{cm}^{-1}$, at 180°C (Table 1). This material also showed a remarkable high performance in PEMFC and DMFC under operation conditions.

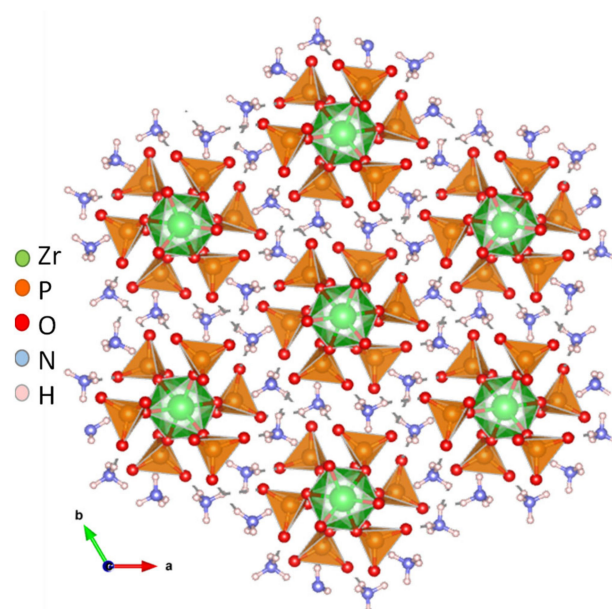


Figure 4. Views of chain packing and H-bond network (dashed grey lines) in compound $(\text{NH}_4)_3\text{Zr}(\text{H}_{2/3}\text{PO}_4)_3$ (adapted from [55]).

2.2. Zirconium Phosphate Composite Membranes

ZrP has been widely studied as a suitable filler for the preparation of Nafion[®]-composite electrolytes due to its good thermal and chemical stability, proton conductivity, hydrophilic nature, very low toxicity, and stability in hydrogen/oxygen atmospheres.

Nafion[®], a sulfonated tetrafluoroethylene-based fluoropolymer copolymer is the most widely used proton conductor for polymer electrolyte membrane fuel cells (PEMFCs) [56].

Despite its excellent properties, this polymer is limited to operations at low temperatures of <100 °C, due to dehydration, which drastically reduces the proton conductivity. As operating at higher temperatures is desirable for better efficiency, Nafion[®] composite membranes have been investigated in which fillers of diverse nature were incorporated to the polymer using different approaches.

Various methodologies of preparing Nafion[®]/ZrP membranes have been devised [46,57–65]. Among them, treatment of the Zr(IV)-exchanged ionomer with phosphoric acid [59], filler/ionomer co-precipitation [61] and casting of ionomer solution/filler gel mixtures [60–62]. In general, improvements in mechanical properties and efficiency [61] were highlighted, although high filler loads beyond 25% led to decreased proton conductivity in certain cases.

A derivation of the above methods consisted of using nanosized ZrP particles-containing ionomer Aquivion[®] as fillers [63]. The resulting composite membranes showed enhanced elastic modulus and lower proton conductivity as compared to Nafion[®] itself, although they were high enough for fuel cell application [64] with values ranging between 0.16 and 0.23 S·cm⁻¹ at 90% RH [62,65].

Derivatizing ZrP with hydrophobic groups resulted in composite membranes mechanically stronger than the pristine Nafion[®] membrane while displaying high proton conductivities [66–70]. Furthermore, integrating both hydrophobic and hydrophilic ZrP nanofillers showed a synergistic effect with mechanical reinforcement of the composite membrane and better fuel cell performance than that found when single ZrP filler were employed [60]. Other ionomer alternatives to Nafion[®], such as sulfonated poly(arylene ether) and poly(ether ether ketone) polymers (SPAEK and SPEEK, respectively), polybenzimidazole (PBI), and vinyl-type (PVA and PVP), have been employed as components of polymer electrolyte membranes [71].

The sulfonated poly(fluorenyl ether ketone) (SPFEK) polymer presents acceptable proton conductivity and stability; however, its performance is lesser in comparison to the benchmark Nafion[®] ionomer. To overcome this handicap, several approaches have been implemented, one of them being hybridization with α -zirconium phosphate. Recently, SPFEK/ZrP-SO₃H composite membranes have been reported with improved proton conductivity, oxidative stability, methanol cross-over barrier and improved H₂/O₂ fuel cell performance [72,73].

ZrP has been also used as a filler in other polymeric matrices, such as poly(vinylidene fluoride) (PVDF) and (sulfonated poly(styrene-block-(ethylene-ran-butylene)-block-styrene) (S40). The resulting composite membranes were tested for potential applications in DMFC, with improved performance especially relative to reducing the methanol permeability [72,74]. PA-PBI/Zr(HPO₃) composite membranes (PA-PBI = phosphoric acid-doped polybenzimidazole) exhibited enhanced proton conductivity as compared to a pristine polymer electrolyte membrane at 200 °C and 5% RH [75].

A different approach is based on the substitution of the polymer membranes for others more eco-friendly, inexpensive, and biodegradable materials. Although poly(vinyl alcohol) (PVA) is a suitable candidate for this purpose, it still requires some enhancements related to its ionic conductivity due to its rigid structure. As an example, Gouda et al. [76] doped iota carrageenan (IC)/sulfonate PVA (SPVA) membranes with different loads of zirconium phosphates. Enhancement of the membrane properties was attributed to abundant hydrogen bond interactions established between the zirconium phosphate particles and the polymers.

2.3. Titanium and Tin(IV) Phosphates

Structurally, titanium(IV) phosphates are more diverse than ZrP, given that structures containing an oxo/hydroxyl ligand or mixed-valence (Ti^{III}/Ti^{IV}) titanium ions have been reported. In addition to the zirconium phosphate analogues, α - [77] and γ -TiP [78], two more other layered

titanium phosphates, $\text{TiO}(\text{OH})(\text{H}_2\text{PO}_4) \cdot 2\text{H}_2\text{O}$ [79] and $\text{Ti}_2\text{O}_3(\text{H}_2\text{PO}_4)_2 \cdot 2\text{H}_2\text{O}$ are known [80]. Furthermore, the mixed-valence titanium phosphate $\text{Ti}^{\text{III}}\text{Ti}^{\text{IV}}(\text{HPO}_4)_4 \cdot \text{C}_2\text{N}_2\text{H}_9 \cdot \text{H}_2\text{O}$ contains microporous channels [81], where monoprotonated ethylenediamine and lattice water are accommodated, which favours its transformation into a porous phase, $\text{Ti}_2(\text{HPO}_4)_4$, at 600 °C with a 3D structure similar to that of $\tau\text{-Zr}(\text{HPO}_4)_2$ [82].

Impedance spectroscopy experiments combined with dynamics simulations revealed that this compound was a good proton conductor, with a σ value of $1.2 \times 10^{-3} \text{ S}\cdot\text{cm}^{-1}$ (at room temperature and 95% RH) and E_a of 0.13 eV (Table 1). From these data, a water-mediated proton transport originating from the H-bond interaction of water molecules with the bridging oxygen of the porous framework was proposed [83].

The crystal structure of two other open-frameworks $\text{Ti}_2\text{O}(\text{PO}_4)_2 \cdot 2\text{H}_2\text{O}$ polymorphs ($\rho\text{-TiP}$ and $\pi\text{-TiP}$) has been reported [84,85]. Fibrous $\rho\text{-TiP}$ and $\pi\text{-TiP}$ crystallize in triclinic and monoclinic unit cells, respectively, and are composed of TiO_6 and $\text{TiO}_4(\text{H}_2\text{O})_2$ octahedra bridged through the orthophosphate groups (Figure 5). This type of connectivity creates two types of 1D channels running parallel to the direction of the fibre growth [84–86]. ^{31}P MAS-NMR spectroscopy studies revealed that $\pi\text{-TiP}$ has capability of adsorbing superficially protonated phosphate species ($\text{H}_3\text{PO}_4/\text{H}_2\text{PO}_4^-/\text{HPO}_4^{2-}$), which affects the proton conductivity properties as confirmed by AC impedance measurements.

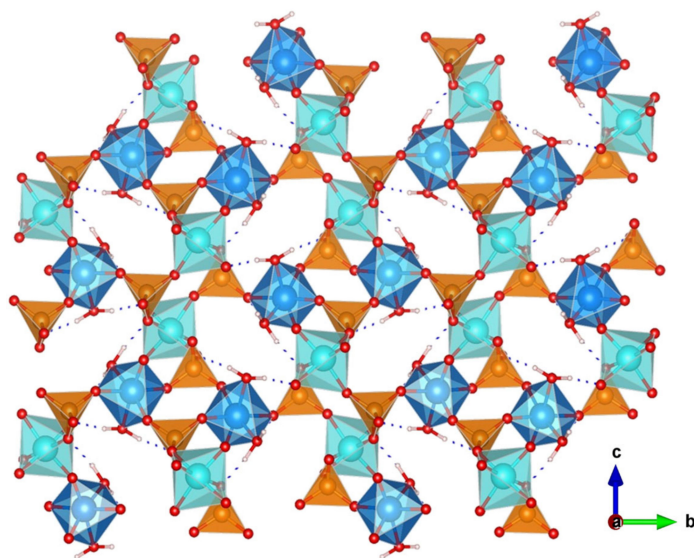


Figure 5. Structure of $\text{Ti}_2\text{O}(\text{PO}_4)_2 \cdot 2\text{H}_2\text{O}$, a fibrous compound with capability of enhancing surface proton transport by H_3PO_4 impregnation (adapted from [86]).

Thus, this solid reached a proton conductivity value of $1.3 \times 10^{-3} \text{ S}\cdot\text{cm}^{-1}$, at 90 °C and 95% RH (Table 1). This behaviour was explained as being due to an extrinsic vehicle-type proton transport mechanism. Additionally, H_3PO_4 -impregnated $\pi\text{-TiP}$ solid was used as filler for the preparation of composite membranes of Chitosan (CS) matrices exhibiting a proton conductivity of $4.5 \times 10^{-3} \text{ S}\cdot\text{cm}^{-1}$ at 80 °C and 95% RH, which is 1.8-fold higher than that of the pristine CS membrane [86].

Insights in the structure of the isomorphous series of layered α -metal(IV) phosphates [$\text{M}(\text{IV}) = \text{Zr}, \text{Ti}, \text{Sn}$] showed appreciable differences in the hydrogen bond interaction of the lattice water with the layers, associated with a variable layer corrugation degree along the series; $\alpha\text{-TiP}$ and $\alpha\text{-SnP}$ displaying H-bonds stronger than the prototype $\alpha\text{-ZrP}$ [87], which, in turn, might have significant implications in making internal surfaces accessible to proton conduction paths.

Nevertheless, studies on structure–property correlations are still lacking, due, in part, to appreciable differences in chemical stability under different conditions, particularly in the case of $\alpha\text{-SnP}$. Recent studies carried out on a nanolayered γ -type tin phosphate,

$\text{Sn}(\text{HPO}_4)_2 \cdot 3\text{H}_2\text{O}$, have revealed that this solid could be obtained in a water-delaminated form, which showed a high proton conductivity of $\sim 1 \times 10^{-2} \text{ S}\cdot\text{cm}^{-1}$ at 100°C and 95% RH (Table 1). This high value was attributed to strong H-bonds between water and the SnP layers, in combination with a high surface area of $223 \text{ m}^2\cdot\text{g}^{-1}$ [88].

2.4. Other Tetravalent Phosphates

POH groups-containing silicophosphates have received attention as proton-conducting electrolytes [42] but its solid-state structural characterization is elusive, at least, under conditions similar to those used in operating fuel cells [89]. A conductivity value of $2.5 \times 10^{-3} \text{ S}\cdot\text{cm}^{-1}$ at 180°C , under more than 0.4% RH, was reported for a silicophosphate-based composite membrane. However, it was noted that the formation of $\text{Si}_5\text{O}(\text{PO}_4)_6$ crystals, under dry conditions, was detrimental for the proton conductivity.

NASICON-type compounds with the general formula, $\text{A}_x\text{B}_2(\text{PO}_4)_3$, where $\text{A} = \text{H}^+, \text{H}_3\text{O}^+$, or NH_4^+ and $\text{B} = \text{Zr}, \text{Ti}, \text{Hf}, \text{Sn}, \text{Ge}$, etc., are also potential proton conductors [90,91]. $\text{HZr}_2(\text{PO}_4)_3$ was firstly prepared by Clearfield et al. [92] and Komorowski et al. [93] described the synthesis of a hydrogen form from $\text{Na}_{1+x}\text{Zr}_2\text{Si}_x\text{P}_{3-x}\text{O}_{12}$ by replacing Na^+ ions with hydronium ions through ion exchange. This solid showed a bulk proton conductivity of $5.0 \times 10^{-4} \text{ S}\cdot\text{cm}^{-1}$ at 100% RH and 25°C , the proton transport mechanism being a Grotthuss-type one [93].

Other materials, such as $\text{HZr}_2(\text{PO}_4)_3 \cdot n\text{H}_2\text{O}$, $\text{NH}_4\text{Zr}_2(\text{PO}_4)_3$, or $\text{H}_{1\pm x}\text{Zr}_2\text{M}_x(\text{PO}_4)_3 \cdot \text{H}_2\text{O}$ ($\text{M} = \text{Nb}, \text{Y}$) [94,95], have been reported. Some NASICON-type compounds based on zirconium or titanium hydrogen phosphate exhibit remarkable proton conductivity while showing a high thermal stability, at least for the case of zirconium derivatives [96,97]. Less studied are the NASICON-type hafnium hydrogen phosphates. Among them, $(\text{NH}_4)_{0.4}\text{H}_{0.6}\text{Hf}_2(\text{PO}_4)_3$, obtained by thermal decomposition of the cubic $\text{NH}_4\text{Hf}_2(\text{PO}_4)_3$ at 550°C , showed a proton conductivity of $1.2 \times 10^{-6} \text{ S}\cdot\text{cm}^{-1}$ at 500°C [90].

2.5. Tetravalent Pyrophosphates

In addition to acid metal(IV) phosphates, tetravalent metal pyrophosphates (MP_2O_7 ; $\text{M} = \text{Sn}, \text{Ce}, \text{Ti}, \text{Zr}$), in particular tin(IV) derivatives, have received considerable attention as proton conductors for intermediate temperature electrolyte applications. These solids combine high thermal stability ($T \geq 400^\circ\text{C}$) with conductivities of 10^{-3} – $10^{-2} \text{ S}\cdot\text{cm}^{-1}$ in the temperature range of 100 – 300°C , under anhydrous or low humidity conditions [98–102]. The origin of this proton conductivity was initially explained because of protons being incorporated into the framework, formed by metal(IV) octahedra and corner-sharing phosphate tetrahedral, after interaction with water vapor.

Defect sites, such as electron holes [103] and oxygen vacancies are believed to favour proton generation [104]. These protons may occupy hydrogen-bonding interstitial sites on either the $\text{M}-\text{O}-\text{P}$ or the $\text{P}-\text{O}-\text{P}$ bonds, thus, generating a hopping proton transport between these sites [105,106]. In support of this, ^1H NMR studies revealed two signals corresponding to hydrogen-bonded interstitial protons at phosphate tetrahedral and metal octahedral sites in In^{3+} -doped SnP_2O_7 . Furthermore, indium doping seemed not to affect the proton conduction occurring by a hopping mechanism between octahedral and tetrahedral sites.

Thus, the increased proton conductivity is instead attributable to increased proton concentration [107]. The strategy of dopant insertion into the $\text{M}(\text{IV})$ pyrophosphate has been further extended to include other dopant divalent and trivalent metal ions, such as Mg^{2+} , Al^{3+} , Sb^{3+} , Sc^{3+} , and Ga^{3+} , with a maximum conductivity of $0.195 \text{ S}\cdot\text{cm}^{-1}$ (Table 1) being reported for $\text{In}_{0.1}\text{Sn}_{0.9}\text{P}_2\text{O}_7$ [108]. However, recent studies on metal doped and undoped SnP_2O_7 suggested that it is in co-precipitated phosphorous-rich amorphous phases where the proton conductivity mostly resides, while the crystalline phase exhibit a very low conductivity ($\sim 10^{-8} \text{ S}\cdot\text{cm}^{-1}$ at 150 – 300°C) [109].

Notwithstanding, the proton conductivity of the high temperature-sintered materials could be recovered by phosphoric acid treatment [110] or by carefully choosing

the phosphate precursor. For the latter case, tetrabutylammonium phosphate-based $\text{SnP}_2\text{O}_7/\text{Nafion}^{\text{®}}$ composite membranes showed an increased fuel cell performance, as compared to other analogous $\text{SnP}_2\text{O}_7/\text{Nafion}^{\text{®}}$ composite membranes [111]. A major challenge in using metal(IV) pyrophosphates as electrolytes is forming dense pellets and the associated low open circuit voltages (OCVs) and considerable gas crossover [108].

Several studies to test applicability of composite membranes for ITFCs have been conducted. For this purpose, dispersion of $\text{Sb}_{0.2}\text{Sn}_{0.8}\text{P}_2\text{O}_7$ nanoparticles into H_3PO_4 -doped PBI membranes were shown to exhibit enhanced conductivities and greater power density relative to the pristine membranes in the single cell tests [112]. Similar claims were made for composite membranes based on $\text{Sn}_{0.95}\text{Al}_{0.05}\text{P}_2\text{O}_7$ [113]. Other approaches, such as using graphite oxide (GO)/ SnP_2O_7 or biphosphate-containing $\text{SnP}_2\text{O}_7/\text{Nafion}$ composite membranes have been accomplished.

The former showed improved proton conductivity ($\sim 7.6 \times 10^{-3} \text{ S}\cdot\text{cm}^{-1}$) peak power density of $18 \text{ mW}\cdot\text{cm}^{-2}$ at $220 \text{ }^{\circ}\text{C}$ and reduced fuel crossover [114]. The latter, aimed at increasing stability by establishing strong ammonium cation-biphosphate ion interactions, which prevents the loss of biphosphate and, hence, optimises the three-phase interface at the fuel cell electrodes. With these improvements, the H_2/O_2 fuel cell delivered a power density of $870 \text{ mW}\cdot\text{cm}^{-2}$ at $240 \text{ }^{\circ}\text{C}$, with minimal performance loss even under exposure to gas containing 25% carbon monoxide [37].

Mg-doped cerium pyrophosphate, with optimal composition of $\text{Ce}_{0.9}\text{Mg}_{0.1}\text{P}_2\text{O}_7$, showed a remarkable performance as electrolyte into a fuel cell, generating electricity up to $122 \text{ mA}\cdot\text{cm}^{-2}$ at 0.33 V and displaying a peak power value of $40 \text{ mW}\cdot\text{cm}^{-2}$ when using 50% H_2 at $240 \text{ }^{\circ}\text{C}$. Prepared in disk form and sintered at $450 \text{ }^{\circ}\text{C}$, the Mg-doped material exhibited a significantly high proton conductivity in the presence of moist air ($P_{\text{H}_2\text{O}} = 0.114 \text{ atm}$) between 160 and $280 \text{ }^{\circ}\text{C}$. A maximum value of $4.0 \times 10^{-2} \text{ S}\cdot\text{cm}^{-1}$ was found at $200 \text{ }^{\circ}\text{C}$, (Table 1), which was even higher than that of CeP_2O_7 ($3.0 \times 10^{-2} \text{ S}\cdot\text{cm}^{-1}$, at $180 \text{ }^{\circ}\text{C}$) [115].

Low crystallinity titanium pyrophosphates also exhibit high proton conductivity [116]. Values of 0.0019 – $0.0044 \text{ S}\cdot\text{cm}^{-1}$, at $100 \text{ }^{\circ}\text{C}$ and 100% RH were reported for these compounds. The proton conduction is attributable to the presence of H_2PO_4^- and HPO_4^{2-} species, demonstrated by ^{31}P MAS NMR and FTIR, and it occurs through a water-facilitated Grotthuss-type proton transport mechanism. Titanium phosphates are also prone to be functionalized with phosphonates groups. Thus, mixed titanium phosphate/phosphonates, $\text{Ti}(\text{HPO}_4)_{1.00}(\text{O}_3\text{PC}_6\text{H}_4\text{SO}_3\text{H})_{0.85}(\text{OH})_{0.30}\cdot n\text{H}_2\text{O}$ [117], displayed an exceptional proton conductivity of $0.1 \text{ S}\cdot\text{cm}^{-1}$ at $100 \text{ }^{\circ}\text{C}$ (Table 1).

A structurally different proton-conductor metal pyrophosphate is the mixed template-containing vanadium nickel pyrophosphate, $(\text{C}_6\text{H}_{14}\text{N}_2)[\text{NiV}_2\text{O}_6\text{H}_8(\text{P}_2\text{O}_7)_2]\cdot 2\text{H}_2\text{O}$ (Figure 6). Its crystal structure is composed of octahedrally coordinated V(IV) and Ni(II) interconnected through bridging pyrophosphate groups, thus creating a 3D framework of $[\text{NiV}_2\text{O}_6\text{H}_8(\text{P}_2\text{O}_7)_2]^{2-}$ unit charged-compensated by protonated DABCO molecules. Hydrogen-bonding networks inside 3D channels facilitate the proton transport, and thus this material exhibits a remarkable proton conductivity of $2.0 \times 10^{-2} \text{ S}\cdot\text{cm}^{-1}$ at $60 \text{ }^{\circ}\text{C}$ and 100% RH (Table 1) through a Grotthuss-type proton-transfer mechanism ($E_a = 0.38 \text{ eV}$) [118].

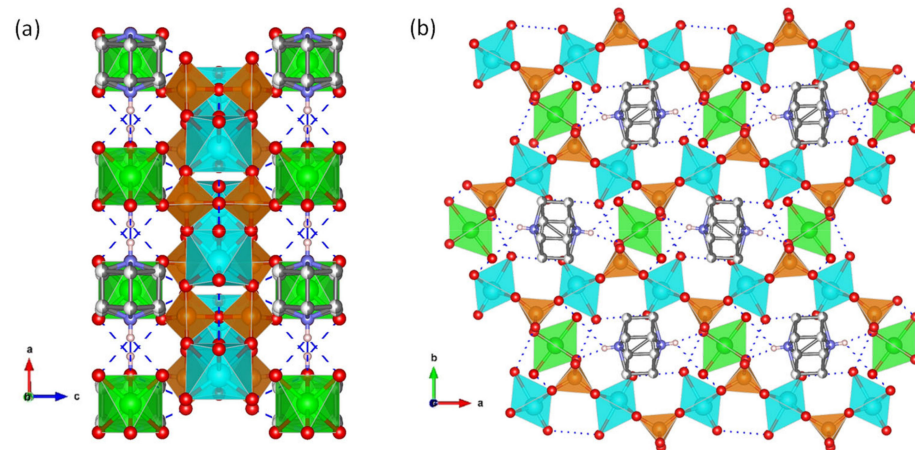


Figure 6. (a) View, along *b*-axis, of the chain packing and (b) 3D-framework of compound $(\text{NH}_4)_3\text{Zr}(\text{H}_{2/3}\text{PO}_4)_3$, with H-bond network (dashed blue lines) highlighted (adapted from [118]).

3. Super Protonic Metal(I) Phosphates

Solid acid proton conductors, with stoichiometry $\text{M}^{\text{I}}\text{HyXO}_4$ ($\text{M}^{\text{I}} = \text{Cs, Rb}$; $\text{X} = \text{S, P, Se}$; $y = 1, 2$), have received much attention because they exhibit exceptional proton transport properties and can be used as electrolytes in fuel cells operated at intermediate temperatures (120–300 °C). The fundamental characteristics of these materials are the phase transition that occurs in response to heating, cooling or application of pressure [6,119], accompanied by an increase in proton conductivity of several orders of magnitude—referred to as *super protonic* conductivity (Figure 7).

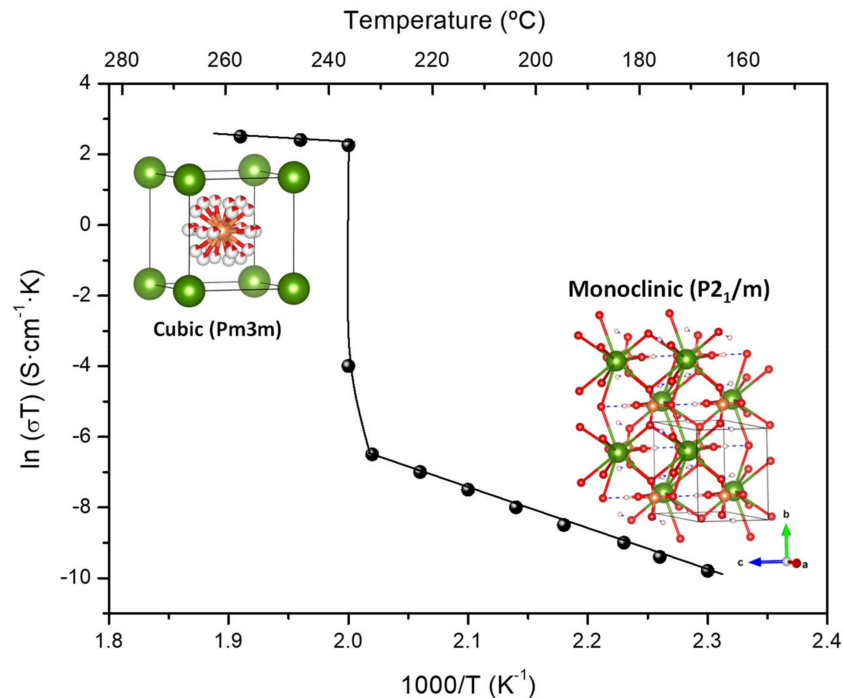


Figure 7. The characteristic high and low temperature proton conductivity and the corresponding structures for CsH_2PO_4 , adapted from [6,120].

This property has been associated with the delocalization of hydrogen bonds [120]. For CsH_2PO_4 , a proton conductivity of $6 \times 10^{-2} \text{ S}\cdot\text{cm}^{-1}$ (Table 1) was measured above 230 °C corresponding to the *super protonic* cubic (*Pm*–3*m*) phase [121] while it drastically drops in the low temperature phases. Recently, from an *ab initio* molecular dynamics

simulation study of the solid acids CsHSeO₄, CsHSO₄ and CsH₂PO₄, it was concluded that efficient long-range proton transfer in the high temperature (HT) phases is enabled by the interplay of high proton-transfer rates and frequent anion reorientation.

In these compounds, proton conduction follows a Grotthuss mechanism with proton transfer being associated with structural reorientation [122]. The *super protonic* conductor CsH₂PO₄ is stable under humidified conditions ($P_{\text{H}_2\text{O}} = 0.4$ atm) [6], but it dehydrates to CsPO₃, via the transient phase Cs₂H₂P₂O₇, at 230–260 °C, according to the relationship $\log(P_{\text{H}_2\text{O}}/\text{atm}) = 6.11(\pm 0.82) - 3.63(\pm 0.42) \times 1000/(T_{\text{dehy}}/\text{K})$ [123].

Several studies [6,124,125] have shown that CsH₂PO₄ can be employed as the electrolyte in fuel cells with good long-term stability. Thus, a continuous, stable power generation for both H₂/O₂ and direct methanol fuel cells operated at ~240 °C was demonstrated for this electrolyte when stabilized with water partial pressures of ~0.3–0.4 atm. In fact, high performances, corresponding to single cell peak power densities of 415 mW·cm^{−2}, was achieved for a humidified H₂/O₂ system provided with a CsH₂PO₄ electrolyte membrane of only 25 μm in thickness [126].

Various strategies, including salt modification by cation and anion substitution [127–130], and mixing with oxide materials [131–137] or organic additives [121,138–140], have been explored to improve the solid acid performance. The preparation of these derivatives and composites involved different synthesis techniques, such as sol-gel, impregnation, thin-casting and electrospinning, depending on the state of the precursor materials and the desired product [6].

Studies on the effects of incorporating different substituents in the structure of CsH₂PO₄ have shown mixed results. Thus, while incorporation of Rb⁺, up to 19%, led to a maximum conductivity of 0.03 S·cm^{−1}, at 240 °C, Ba²⁺-doping only increased the conductivity of the low temperature phase in two orders of magnitude [127]. On the other hand, substitution of phosphorus with Mo or W hardly modified the proton conductivity, as compared to the parent compound. For S-doping, a shift to lower temperatures of the phase transition was observed at low S-contents, while the conductivity increased only for the low temperature phase.

Mixing CsH₂PO₄ with H₃PO₄ or CsH₅(PO₄)₂ resulted in composites Cs_{1−x}H_{2+x}PO₄ ($x_{\text{mole}} = 0.01–0.05$) with excesses of protons. In comparison with CsH₂PO₄, these composites exhibited super protonic phase transition at lower temperature (up to ~200 °C) and increased lower-temperature conductivities ($\sigma_{150\text{ °C}} \sim 2 \times 10^{-3}$ S·cm^{−1}, $x = 0.1$) [141]. Addition of Cs₂HPO₄·2H₂O to CsH₂PO₄ (up to an $x_{\text{mole}} = 0.03$) also resulted in an enhanced low-temperature conductivity and decreased the activation energy to $E_a = 0.56$ eV. For all these composites no significant changes in the high-temperature conductivity were observed, although the super protonic phase transition became more diffuse and almost disappeared in some case [141,142].

Improvements in the mechanical and proton conductivity properties, as well as in thermal stability of CsH₂PO₄-based electrolytes have been addressed by mixing with oxide materials, such as zirconia, silica, alumina, and titania (Table 1). Thus, the (1−x)Cs₃(HSO₄)₂(H₂PO₄)/xSiO₂ composite with $x = 0.7$ increase the proton conductivity up to 10^{−2} S·cm^{−1} in the range 60–200 °C. Moreover, the introduction of fine-particle silica reduced the jump in conductivity at the phase-transition temperature and shifted it to lower temperatures. Higher silica contents led to a decrease in the conductivity due to the disruption of conduction paths [132].

The use of acid-modified silica confers high thermal stability at low H₂O partial pressure while maintaining high proton conductivity (10^{−3}–10^{−2} S·cm^{−1}, at 130–250 °C) [134]. A similar trend was found for the composites (1−x)CsH₂PO₄/xTiO₂ and (1−x)CsH₂PO₄/xZrO₂ (contents $x = 0.1$ and 0.2) [135,136]. High performance was also reported for the composite 8:1:1 CsH₂PO₄/NaH₂PO₄/ZrO₂, with a stable conductivity of 2.23×10^{-2} S·cm^{−1} for 42 h being measured for the high temperature phase [137]. Nanodiamonds (ND) are another type of heterogeneous additive giving rise to the (1−x)CsH₂PO₄-xND ($x = 0–0.5$)

composites exhibiting enhanced low temperature proton conductivities, while maintaining almost unaltered that of high temperature [140].

CsH₂PO₄ composites based on organic additives have been also intensively investigated. For example, binary mixtures containing N-heterocycles (1,2,4-triazole, benzimidazole and imidazole) displayed enhanced proton conductivity at temperatures below the super protonic phase transition ($2 - 8 \times 10^{-4} \text{ S}\cdot\text{cm}^{-1}$ at 174–190 °C) [138]. Another approach was reported in which the solid acid CsH₂PO₄ was combined with fluoroelastomer p(VDF/HFP), producing high conductive composite membranes (1-x)CsH₂PO₄-xp(VDF/HPF) (x = 0.05–0.25 wt%) with improved mechanical and hydrophobic properties, along with flexibility and reduced thickness.

However, a high concentration of p(VDF/HFP) rendered membranes with a reduced proton conductivity for the HT phase [141]. By using the polymer butvar (polyvinyl butyral) [121], composite membranes (1-x)CsH₂PO₄-xButvar (x < 0.2 wt%) were obtained showing, in a wide range of composition, a proton conduction behaviour analogous to the pure salt in the high temperature region but with increased low temperature conductivity by three orders of magnitude at x = 0.2.

Table 1. Proton conductivity data for selected monovalent and tetravalent metal phosphates and pyrophosphates.

Compounds/Dimensionality	Temperature (°C)/RH(%)	Conductivity (S·cm ⁻¹)	Ea (eV)	Ref.
<i>Tetravalent Metal Phosphates</i>				
ZrP·0.8PrNH ₂ ·5H ₂ O/2D	20/90	1.2×10^{-3}	1.04	[50]
Zr(P ₂ O ₇) _{0.81} (O ₃ POH) _{0.38} /2D	20/90	1.3×10^{-3}	0.19	[51]
Zr(O ₃ POH) _{0.65} (O ₃ PC ₆ H ₄ SO ₃ H) _{1.35} /2D	100/90	7.0×10^{-2}	—	[52]
(NH ₄) ₂ [ZrF ₂ (HPO ₄) ₂]/3D	90/95	1.45×10^{-2}	0.19	[53]
(NH ₄) ₅ [Zr ₃ (OH) ₃ F ₆ (PO ₄) ₂ (HPO ₄)]/3D	60/98	4.41×10^{-2}	0.33	[54]
(NH ₄) ₃ Zr(H ₂ / ₃ PO ₄) ₃ /1D	90/95	1.21×10^{-2}	0.30	[55]
Ti ₂ (HPO ₄) ₄ /1D	20/95	1.2×10^{-3}	0.13	[83]
Ti ₂ O(PO ₄) ₂ ·2H ₂ O (π-TiP)/3D	90/95	1.3×10^{-3}	0.23	[86]
Ti(HPO ₄) ₁ (O ₃ PC ₆ H ₄ SO ₃ H) _{0.85} (OH) _{0.30} ·nH ₂ O/2D	100/—	0.1	0.18	[117]
Sn(HPO ₄) ₂ ·3H ₂ O/2D	100/95	1.0×10^{-2}	—	[88]
α-ZrP ₂ O ₇ /3D	300	1.0×10^{-4}	—	[49]
(NH ₄) ₃ Zr(H ₂ / ₃ PO ₄) ₃ /1D	180	1.45×10^{-3}	0.26	[55]
<i>Tetravalent Pyrophosphates</i>				
TiP ₂ O ₇ /3D	100/100	4.4×10^{-3}	0.14	[116]
(C ₆ H ₁₄ N ₂)[NiV ₂ O ₆ H ₈ (P ₂ O ₇) ₂]·2H ₂ O/3D	60/100	2.0×10^{-2}	0.38	[118]
In _{0.1} Sn _{0.9} P ₂ O ₇ /3D	300	0.195	—	[108]
Ce _{0.9} Mg _{0.1} P ₂ O ₇ /3D	200	4.0×10^{-2}	—	[115]
CeP ₂ O ₇ /3D	180	3.0×10^{-2}	—	[115]
<i>Super protonic Cesium Phosphates</i>				
CsH ₂ PO ₄ /3D	>230	6.0×10^{-2}	—	[120]
Cs _{1-x} Rb _x H ₂ PO ₄ /3D	240	3.0×10^{-2}	0.92	[127]
Cs _{1-x} H _{2+x} PO ₄ /3D	150	2.0×10^{-2}	0.70	[141]
(1-x)Cs ₃ (HSO ₄) ₂ (HPO ₄)/xSiO ₂	200	1.0×10^{-2}	—	[132]
(1-x)CsH ₂ PO ₄ /xTiO ₂	230	2.0×10^{-2}	—	[135]
(1-x)CsH ₂ PO ₄ /xZrO ₂	250	2.6×10^{-2}	—	[136]
CsH ₂ PO ₄ /NaH ₂ PO ₄ /ZrO ₂	230	2.23×10^{-2}	—	[137]

4. Divalent and Trivalent Metal Phosphates

4.1. Divalent Metal Phosphates

Divalent transition metal phosphates show a great structural versatility, from 1D polymeric topologies through layered framework to 3D open-framework structures. Most of these solids are synthesized in the presence of organic molecules, which are retained as protonated guest species (amines, iminazole derivatives, etc.), thus, compensating the anionic charge of the inorganic framework. This is formed by the metal ion, mainly in octahedral or tetrahedral coordination environments, linked to the phosphate groups with different protonated degrees (H_xPO_4). The presence of the latter makes possible the formation of effective and extensive hydrogen bond networks with participation of water molecules. In addition, protonated guest species and water itself can act as proton carriers, thus, boosting proton conduction (Table 2) [12–14].

Several 3D open-framework M(II) phosphates have been reported [14,143], which consist of $[CoPO_4]_{\infty}^-$ or $[Zn_2(HPO_4)_2(H_2PO_4)_2]^{2-}$ anionic frameworks that contain organic charge-compensating ions in their internal cavities. $(C_2N_2H_{10})_{0.5}CoPO_4$ exhibited negligible conductivity in anhydrous conditions; however, it displayed a relatively high water-mediated proton conductivity $2.05 \times 10^{-3} S \cdot cm^{-1}$ at 56 °C and 98% RH. On the other hand, the solid $NMe_4 \cdot Zn[HPO_4][H_2PO_4]$ experiences a structural transformation from monoclinic (α) to orthorhombic (β) upon heating at 149 °C. Both polymorphs contain 12-membered rings composed of tetrahedral Zn^{2+} ions linked to protonated phosphate groups without changing Zn-O-P connectivity (Figure 8).

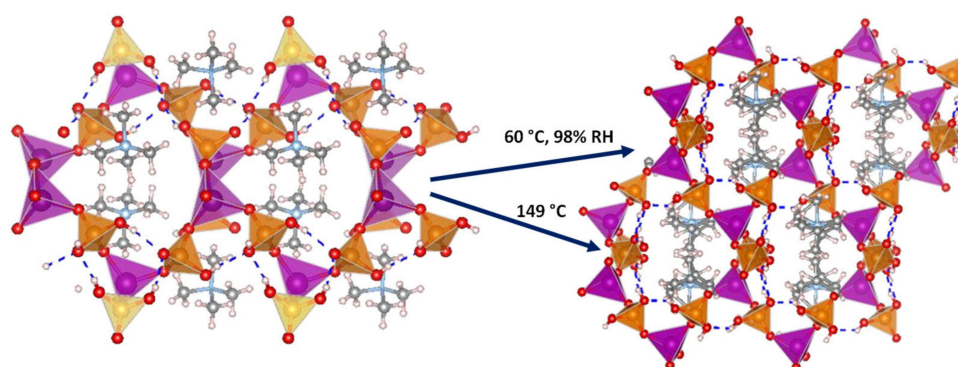


Figure 8. Irreversible structural transformation in $NMe_4Zn[HPO_4][H_2PO_4]_4$ adapted from [143]. N (sky-blue), O (red), Zn (magenta), P (orange), C (grey) and H (pale pink) atoms.

The α phase transforms into the β phase at high humidity and temperatures above 60 °C, and then reaches a proton conductivity of $1.30 \times 10^{-2} S \cdot cm^{-1}$ at 98% RH, a behaviour that might be attributed to the participation of adsorbed water molecules in creating H-bonding networks with effective pathways for proton conduction. The conductivity drastically decreases at 65 °C. In anhydrous conditions, the α phase exhibited a proton conductivity of $\sim 10^{-4} S \cdot cm^{-1}$ at 160 °C, similar values were found for other reported zinc phosphates at temperatures between 130 and 190 °C [12,144,145].

Membrane-electrode assembly prepared with the pelletized solid, gave an observed open circuit voltage (OCV) of 0.92 V at 190 °C measured in a H_2 /air cell, suggesting that the dominant conductive species are protons, and the proton transport from anode to cathode takes place through H-bond networks in the pellet.

As an example of 2D metal phosphate water-assisted proton conductors, $(C_2H_{10}N_2)[Mn_2(HPO_4)_3](H_2O)$, displayed a proton conductivity of $1.64 \times 10^{-3} S \cdot cm^{-1}$ under 99% RH at 20 °C. This proton conductivity was attributed to the formation of dense H-bond networks in the lattice, composed of Mn_3O_{13} units-containing anionic layers [146], which provide efficient proton-transfer pathways for a Grotthuss-type proton transport at high RH.

Another way of improving the proton conductivity in layered divalent metal phosphates is favouring the formation of hydrogen bond networks by ion exchange. For instance [17], partial exchange of Na^+ for ethylenediammonium yielded two new crystalline phases, with composition $(\text{C}_2\text{H}_{10}\text{N}_2)_x\text{Na}_{1-x}[\text{Mn}_2(\text{PO}_4)_2]$ ($x = 0.37$ y 0.54), which influenced formation of extended hydrogen bond networks and concomitant increase in proton conductivity, from $2.22 \times 10^{-5} \text{ S}\cdot\text{cm}^{-1}$ for the as-synthesized material (in ethylenediammonium form) to $1.3 \times 10^{-2} \text{ S}\cdot\text{cm}^{-1}$ ($x = 0.37$) and $2.1 \times 10^{-2} \text{ S}\cdot\text{cm}^{-1}$ ($x = 0.54$) at 99% RH and 30 °C.

This strategy of enhancing proton conductivity was further extended successfully to other 2D manganese phosphates [18]. A proton conductivity value as high as $7.72 \times 10^{-2} \text{ S}\cdot\text{cm}^{-1}$ was reached at 30 °C and 99% RH for K^+ -exchanged compounds, which compares well with those of MOF-based open-framework materials [147–149]. The 1D solid $[\text{Zn}_3(\text{H}_2\text{PO}_4)_6(\text{H}_2\text{O})_3](\text{Hbim})$ (Hbim= benzimidazole) prepared by mechanochemical synthesis is characterized by presenting a dual-function as proton conductor.

It loses the coordinated water by heating transforming into $[\text{Zn}_3(\text{HPO}_4)_6](\text{Hbim})$, which exhibits an intrinsic proton conductivity higher than the hydrated form, reaching a value of $1.3 \times 10^{-3} \text{ S}\cdot\text{cm}^{-1}$ at 120 °C, believed to be due to a rearrangement of the conduction path and the liquid-like behaviour of benzimidazole molecules. In addition, this solid also showed porosity, thus, enabling the adsorption of gaseous methanol that further improved the proton conductivity of the anhydrous phase. This enhancement of proton conductivity in methanol-adsorbed samples was explained by the effective participation of the guest molecule in formation of extended hydrogen-bond interactions [19].

An ordered-to-disordered structural transformation and its implication in proton conduction were investigated for the 1D copper phosphate $[\text{ImH}_2][\text{Cu}(\text{H}_2\text{PO}_4)_2\text{Cl}]\cdot\text{H}_2\text{O}$ (Im = imidazole). In this structure, the protonated imidazole (ImH_2) and the water molecule are located in interspaces of the anionic chains $[\text{Cu}(\text{H}_2\text{PO}_4)_2\text{Cl}]^-$. Upon heating a structural transformation from an ordered crystalline state to a disordered state occurred. Highly mobile and structurally disordered H^+ carriers were supposed to be responsible of the high proton conductivity $2 \times 10^{-2} \text{ S}\cdot\text{cm}^{-1}$ at 130 °C, under anhydrous conditions [150].

A 1D zinc phosphate-based proton conductor, $[\text{Zn}_3(\text{H}_2\text{PO}_4)_6(\text{H}_2\text{O})_3](\text{BTA})$ (BTA = 1,2,3-benzotriazole) has been reported [151] that exhibits high proton conductivity, $8 \times 10^{-3} \text{ S}\cdot\text{cm}^{-1}$ in anhydrous glassy-state (120 °C). The glassy-state, developed via melt-quenching, was suggested to induce isotropic disordered domains that enhanced H^+ dynamics and conductive interfaces. In fact, the capability of the glassy-state material as an electrolyte was found suitable for the rechargeable all-solid-state H^+ battery operated in a wide range of temperatures from 25 to 110 °C.

Focus has been also put on metal phosphate-based solid solutions [152,153]. Vacancies can be generated that introduce extra protons into the structure and increase the proton conduction. This effect was investigated for the 1D rubidium and magnesium polyphosphate compound, $\text{RbMg}_{1-x}\text{H}_{2x}(\text{PO}_3)_3\cdot y\text{H}_2\text{O}$, for which system a maximum proton conductivity of $5.5 \times 10^{-3} \text{ S}\cdot\text{cm}^{-1}$ was measured at 170 °C with a vehicle-type mechanism of H_3O^+ conduction.

The proton conductivity results from H-bond interactions between water molecules and corner-sharing PO_4 chains that provide formation of sandwiched edge-sharing RbO_6 - MgO_6 chain [152]. Another example is the solid solution with composition $\text{Co}_{1-x}\text{Zn}_x(\text{H}_2\text{PO}_4)_2\cdot 2\text{H}_2\text{O}$ ($0 < x < 1.0$), which showed the highest conductivity value, $2.01 \times 10^{-2} \text{ S}\cdot\text{cm}^{-1}$ at 140 °C, for a composition $\text{Co}_{0.5}\text{Zn}_{0.5}(\text{H}_2\text{PO}_4)_2\cdot 2\text{H}_2\text{O}$ [153].

4.2. Trivalent Metal Phosphates

Zeolite-like open framework metal(III) phosphates consist of metal(III) ions-phosphate species (PO_4^{3-} , HPO_4^{2-} , H_2PO_4^-) linkages featuring internal cavities, where charge-compensating cations and/or neutral species are located and, thus, dense hydrogen bond networks frequently result. In addition, the robust inorganic framework endues this porous

material with better thermal and chemical stability compared with porous coordination polymers/metal organic frameworks (PCPs/MOFs) [13].

Regarding to proton conductivity (Table 2), aluminium phosphate-based solids are by far the most studied compounds [154–167]. The species inside channels affect in different ways to proton conduction. Thus, while water adsorption is key to assist proton transfer in $(\text{NH}_4)_2\text{Al}_4(\text{PO}_4)_4(\text{HPO}_4)\cdot\text{H}_2\text{O}$ by a hopping mechanism along H-bond chains [166], densely packed NH_4^+ ions show negligible contribution because of hampered migration.

By using an organic template-free synthetic methodology, a 3D open-framework aluminophosphate $\text{Na}_6[(\text{AlPO}_4)_8(\text{OH})_6]\cdot 8\text{H}_2\text{O}$ (JU103) was prepared [158], which showed a proton conductivity of $3.59 \times 10^{-3} \text{ S}\cdot\text{cm}^{-1}$, at 20 °C and 98% RH. It was argued that the enhanced conductivity of the as-synthesized material as compared to its NH_4^+ - or Ag^+ -exchanged forms is indicative of a beneficial effect of hydrated Na^+ ions in generating proton-transfer pathways. The 3D cesium silicoaluminophosphate, $\text{Cs}_2(\text{Al}_{0.875}\text{Si}_{0.125})_4(\text{P}_{0.875}\text{Si}_{0.125}\text{O}_4)_4(\text{HPO}_4)$, belonging to the structural family of SAPOs, was shown to exhibit a remarkable proton conductivity of $1.70 \times 10^{-4} \text{ S}\cdot\text{cm}^{-1}$ at low temperature and RH (20 °C and 30%, respectively) [168,169].

Several 2D aluminophosphates have been reported as proton conductors [154,156]. These compounds (denoted as AlPO-CJ70/2) are structurally characterized by displaying an anionic layer: $[\text{Al}_2\text{P}_3\text{O}_{12}]^{3-}$, formed by alternating Al^{3+} and phosphorus tetrahedra, which is charge-compensated by N,N-dimethylbenzylamine or α -methylbenzylamine ions, respectively. In these layered structures, extended H-bond networks are formed through interactions of the amine N atoms, H_2O molecules and protruding phosphate groups of the anionic layer. Consequently, water-mediated proton conduction processes occurred upon immersion in water, with σ values around $10^{-3} \text{ S}\cdot\text{cm}^{-1}$, at 80 °C, and E_a values of 0.16–0.2 eV, typical of a Grotthuss-type proton-transfer mechanism.

By following a synthetic route in which methylimidazolium dihydrogenphosphate was used as a solvent, structure-directing agent, and a phosphorus source, the solid $(\text{C}_4\text{H}_7\text{N}_2)(\text{C}_3\text{H}_4\text{N}_2)_2\cdot\text{Al}_3(\text{PO}_4)_4\cdot 0.5\text{H}_2\text{O}$ (SCU-2) was obtained [164]. Its layered structure, built up from corner-sharing Al^{3+} and P^{V} tetrahedra, features 8-member rings where guest imidazolium ions and water molecules are hosted. At 85 °C and 98% RH, this solid showed a proton conductivity of $5.9 \times 10^{-3} \text{ S}\cdot\text{cm}^{-1}$ and a low activation energy (0.20 eV), characteristic of a Grotthuss-type proton-transfer mechanism. An efficient pathway for the proton transfer was attributed to the hydrogen bond network established between the imidazolium ions and water molecules interacting with the host framework.

A few examples of phosphate-based proton conductors of other trivalent metals do exist. Among them, two Fe(III) phosphates, 1D $(\text{C}_4\text{H}_{12}\text{N}_2)_{1.5}[\text{Fe}_2(\text{OH})(\text{H}_2\text{PO}_4)(\text{HPO}_4)_2(\text{PO}_4)]\cdot 0.5\text{H}_2\text{O}$ [13] and 3D open-framework iron(III) phosphate $(\text{NH}_3(\text{CH}_2)_3\text{NH}_3)_2[\text{Fe}_4(\text{OH})_3(\text{HPO}_4)_2(\text{PO}_4)_3]\cdot 4\text{H}_2\text{O}$ [170], have been reported. Both compounds contain Fe_4O_{20} tetramers as a common structural feature. The 1D solid is composed of chains of tetramers bridged by PO_4^{3-} groups and having terminal H_2PO_4^- and HPO_4^{2-} groups [171], while piperazinium cations and water molecules are disorderly situated in between chains. This arrangement gives rise to extended hydrogen bonding interactions and hence proton conducting pathways. The proton conductivity measured at 40 °C and 99% RH was $5.14 \times 10^{-4} \text{ S}\cdot\text{cm}^{-1}$, and it was maintained upon dispersion of this solid in PVDF [13]. In the case of the 3D solid, infinite chains of interconnected tetramers are interlinked, in turn by phosphate groups that generate large tunnels (Figure 9). The diprotonated 1,3-diaminopropane and water molecules, localized inside tunnels, form an extended hydrogen bond network with the P–OH groups pointing toward cavities. These interactions favour proton hopping, the measured proton conductivity being of $8.0 \times 10^{-4} \text{ S}\cdot\text{cm}^{-1}$, at 44 °C and 99% RH, and with an E_a of 0.32 eV [172]. Furthermore, the proton conductivity of this compound increased up to $5 \times 10^{-2} \text{ S}\cdot\text{cm}^{-1}$ at 40 °C upon exposure to aqua-ammonia vapors from 1 M $\text{NH}_3\cdot\text{H}_2\text{O}$ solution. This result confirms this treatment as an effective way of enhancing proton conductivity, which has been elsewhere demonstrated for the case of coordination polymers [173,174]. The observed variation of E_a with the ammonia concentration also

suggested that NH_3 , as well as H_2O , molecules contribute to create proton-transfer pathways, by a Grotthuss mechanism. However, when ammonia concentrations were lower than 0.5 M, the proton conduction mechanism tended to be vehicle-type one [156].

Table 2. Proton conductivity data for selected divalent and trivalent metal phosphates.

Compounds/Dimensionality	Temperature (°C)/RH(%)	Conductivity ($\text{S}\cdot\text{cm}^{-1}$)	E_a (eV)	Ref.
<i>Divalent Metal Phosphates</i>				
$(\text{C}_2\text{N}_2\text{H}_{10})_{0.5}\text{CoPO}_4/3D$	56/98	2.05×10^{-3}	1.01	[143]
$\text{NMe}_4\cdot\text{Zn}[\text{HPO}_4][\text{H}_2\text{PO}_4]$ (β phase)/3D	60/98	1.30×10^{-2}	0.92	[14]
$(\text{C}_2\text{H}_{10}\text{N}_2)[\text{Mn}_2(\text{HPO}_4)_3](\text{H}_2\text{O})/2D$	20/99	1.64×10^{-3}	0.22	[146]
$(\text{C}_2\text{H}_{10}\text{N}_2)_x\text{Na}_{1-x}[\text{Mn}_2(\text{PO}_4)_2]/2D$	30/99	2.1×10^{-2}	0.14	[17]
$(\text{C}_2\text{H}_{10}\text{N}_2)_{1-x}\text{K}_x[\text{Mn}_2(\text{PO}_4)_2]\cdot 2\text{H}_2\text{O}/2D$	30/99	7.72×10^{-2}	0.18	[18]
$(\text{C}_2\text{H}_{10}\text{N}_2)_{1-x}\text{K}_x[\text{Mn}_2(\text{HPO}_4)_3](\text{H}_2\text{O})/2D$	30/99	0.85×10^{-2}	0.081	[18]
$[\text{Zn}_3(\text{H}_2\text{PO}_4)_6(\text{H}_2\text{O})_3](\text{Hbim})/1D$	120	1.3×10^{-3}	0.50	[19]
$[\text{ImH}_2][\text{Cu}(\text{H}_2\text{PO}_4)_2\text{Cl}]\cdot\text{H}_2\text{O}/1D$	130	2.0×10^{-2}	0.1	[150]
$[\text{Zn}_3(\text{H}_2\text{PO}_4)_6(\text{H}_2\text{O})_3](\text{BTA})/1D$	120	8.0×10^{-3}	0.39	[151]
$\text{RbMg}_{0.9}\text{H}_{0.2}(\text{PO}_3)_3\cdot y\text{H}_2\text{O}/1D$	170	5.5×10^{-3}	—	[152]
$\text{Co}_{0.5}\text{Zn}_{0.5}(\text{H}_2\text{PO}_4)_2\cdot 2\text{H}_2\text{O}/1D$	140	2.01×10^{-2}	—	[153]
<i>Trivalent Metal Phosphates</i>				
$\text{Na}_6[(\text{AlPO}_4)_8(\text{OH})_6]\cdot 8\text{H}_2\text{O}/3D$	20/98	3.59×10^{-3}	0.21	[158]
$[\text{C}_9\text{H}_{14}\text{N}]_8[\text{H}_2\text{O}]_4\cdot[\text{Al}_8\text{P}_{12}\text{O}_{48}\text{H}_4]/2D$	80, in water	9.25×10^{-4}	0.16	[154]
$[\text{R},\text{S}\text{-C}_8\text{H}_{12}\text{N}]_8[\text{H}_2\text{O}]_2\cdot[\text{Al}_8\text{P}_{12}\text{O}_{48}\text{H}_4]/2D$	90/98	3.01×10^{-3}	0.20	[156]
$(\text{C}_4\text{H}_7\text{N}_2)(\text{C}_3\text{H}_4\text{N}_2)_2\cdot\text{Al}_3(\text{PO}_4)_4\cdot 0.5\text{H}_2\text{O}/2D$	85/98	5.94×10^{-3}	0.20	[164]
$\text{In}(\text{HPO}_4)(\text{H}_2\text{PO}_4)(\text{D,L-C}_3\text{H}_7\text{NO}_2)/3D$	85/98	2.9×10^{-3}	0.19	[16]
$(\text{NH}_3(\text{CH}_2)_3\text{NH}_3)_2[\text{Fe}_4(\text{OH})_3(\text{HPO}_4)_2(\text{PO}_4)_3]\cdot 4\text{H}_2\text{O}/1D$	40/99	5.0×10^{-2}	—	[170]

Hbim = benzimidazole; Im = imidazole; BTA = 1,2,3-benzotriazole.

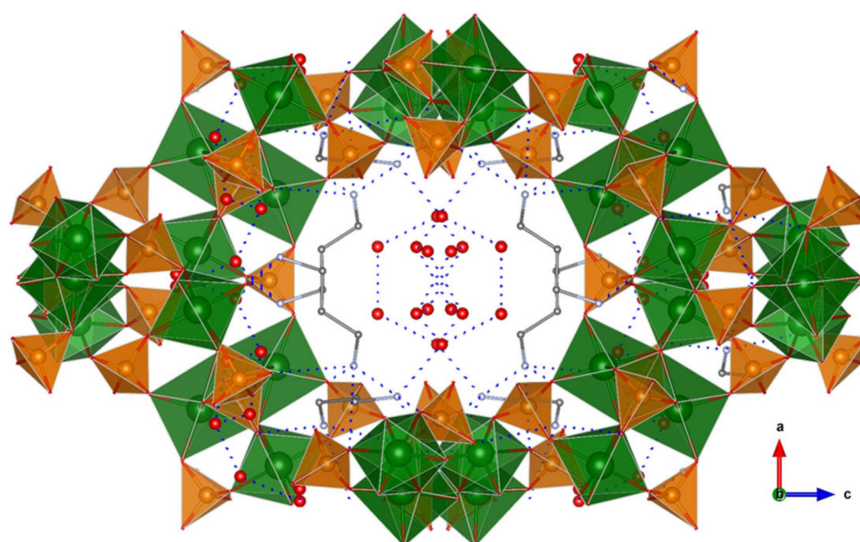


Figure 9. Open-framework structure of $(\text{NH}_3(\text{CH}_2)_3\text{NH}_3)_2[\text{Fe}_4(\text{OH})_3(\text{HPO}_4)_2(\text{PO}_4)_3]\cdot 4\text{H}_2\text{O}$ showing guest species inside channels and H-bond interactions. Fe (green), O (red), P (orange), and C (grey) atoms.

For the series of isostructural imidazole cation (ImH_2)-templated layered metal phosphates, $[\text{ImH}_2][\text{X}(\text{HPO}_4)_2(\text{H}_2\text{O})_2]$ (FJU-25-X, X = Al, Ga, and Fe), it was found that the

proton conductivity was dependent on mobility of imidazole guests, FJU-25-Fe exhibiting the highest proton conductivity ($5.21 \times 10^{-4} \text{ S}\cdot\text{cm}^{-1}$ at 90°C). The determined activation energies ($\sim 0.20 \text{ eV}$) were indicative of a Grotthuss-type mechanism of proton conduction.

The amino acid-template indium phosphate, $\text{In}(\text{HPO}_4)(\text{H}_2\text{PO}_4)(\text{D,L-C}_3\text{H}_7\text{NO}_2)$ (SCU-12), represents a singular example of 3D metal phosphate-based proton conductors [16].

Its crystal structure is formed by edge-sharing four-ring ladders, with the amino acid molecules attached to the ladders through In-O bonds. Further bridging the indium phosphate ladders by the H_2PO_4^- groups gives rise to a three-dimensional structure. The presence of two kinds of proton carriers, H_2PO_4^- ions and zwitterionic alanine molecules, favours the development of high proton conductivities ($2.9 \times 10^{-3} \text{ S}\cdot\text{cm}^{-1}$ at 85°C and 98% RH) through a Grotthuss-type proton-transfer mechanism ($E_a = 0.19 \text{ eV}$).

Other trivalent metal phosphates have been reported, e.g., BPO_x [175] and CePO_4 [176]. The former exhibited a proton conductivity of $7.9 \times 10^{-2} \text{ S}\cdot\text{cm}^{-1}$ as self-supported electrolyte and $4.5 \times 10^{-2} \text{ S}\cdot\text{cm}^{-1}$ as (PBI)-4 BPO_x composite membrane, measured at 150°C and 5% RH, but structure/conductivity correlations were not established because of its amorphous nature. The latter showed a low-temperature (RT) proton conduction $< 10^{-5} \text{ S}\cdot\text{cm}^{-1}$ at 100% RH through a structure-independent proton-transport mechanism [176].

There are only a few examples of metal(III) pyrophosphates displaying proton conductivity. Among them is the open framework magnesium aluminophosphate $\text{MgAlP}_2\text{O}_7(\text{OH})(\text{H}_2\text{O})_2$ (JU102) [167]. Its structure is composed of tetrahedral Al^{3+} and octahedral Mg^{2+} ions coordinated by pyrophosphate ions. This connectivity results in an open framework with unidirectional 8-ring channels. The proton conduction properties originate from the existence of an H-bond network in which coordinated water molecules participate.

Thus, the proton conductivity measured at 55°C on water-immersed samples was $3.86 \times 10^{-4} \text{ S}\cdot\text{cm}^{-1}$ [167], which raised to $1.19 \times 10^{-3} \text{ S}\cdot\text{cm}^{-1}$ when calcined at 250°C and measured at the same conditions, while the E_a value hardly changed from 0.16 to 0.2 eV. This behaviour was explained as being due to a dehydration-rehydration process that enhances proton conductivity by altering the H-bonding network and the pathway of proton transfer.

Another example of 3D open framework metal(III) pyrophosphate is the compound $\text{NH}_4\text{TiP}_2\text{O}_7$ [177]. The structure of this solid is composed of negatively charged $[\text{TiP}_4\text{O}_{12}]^-$ layers, forming one-dimensional six-membered ring channels, where the NH_4^+ ions are located. Its proton conductivity increased from $10^{-6} \text{ S}\cdot\text{cm}^{-1}$ under anhydrous conditions to $10^{-3} \text{ S}\cdot\text{cm}^{-1}$ at full-hydration conditions and 84°C . The low E_a value, 0.17 eV, characteristic of a Grotthuss-type proton-transfer mechanism, was associated with the role played by the NH_4^+ ions in the channels as proton donors and promoters of proton migration. A drop in proton conductivity was observed when the triclinic TiP_2O_7 phase formed by thermal decomposition of $\text{NH}_4\text{TiP}_2\text{O}_7$ [177].

5. Outlook

Great efforts have been devoted to the synthesis and characterization of metal phosphate-based proton conductors over more than three decades. Among them, zirconium phosphates are prominent not only because of the feasibility of Zr(IV) and phosphate ions to form a rich variety of crystallographic architectures (from 1D to 3D open frameworks) but also due to their outstanding properties and workability while being environmentally benign and low cost materials.

Although the prototype layered α -zirconium phosphate has been commonly proven as a filler for PEMFCs devices, new synthetic designs of M(IV) phosphates, including pyrophosphate compounds, are promising candidates to broaden their applicability in different electrochemical devices. Other M(IV) phosphates and pyrophosphates (M = Ti, Sn) are less known due, in part, to their amorphous nature or strong tendency to amorphise

at working temperatures, though, in some cases, these compounds presented remarkable proton conductivity properties.

CsH₂PO₄, a super protonic material, was proven as a suitable electrolyte for both H₂/O₂ and direct methanol fuel cells operated at ~240 °C, and provides excellent performance when controlling its thermal stability. In addition, combinations with other materials are possible to adjust the specific characteristics of the composite CsH₂PO₄ electrolyte, thus, offering a wide range of compositions with tuning properties.

Recently, research and developments in metal phosphate proton conductors have been addressed to divalent or trivalent metal phosphates, which present a remarkable structural versatility and tunable conductivities; however, more in-depth studies are required to assess their potential use and applicability for low and intermediate temperature fuel cells.

Applications of metal phosphates as electrolytes or as electrolyte components are in continuous progress, although their use for energy storage and conversion remains a challenge. For practical applications in fuel cells at low/intermediate temperatures, phosphate-based proton conducting electrolytes have demonstrated acceptable proton conductivity values; however, other features, such as their mechanical strength, chemical/thermal stabilities, film-forming ability (in the case of composite membranes), durability, and fuel cross-over, are key factors to be improved.

Author Contributions: Writing-original draft preparation, R.M.P.C. and M.B.-G.; writing-review and editing, P.O.-P. and A.C. All authors have read and agreed to the published version of the manuscript.

Funding: This research was funded by PID2019–110249RB-I00 (MICIU/AEI, Spain) and PY20–00416 (Junta de Andalucía, Spain/FEDER) research projects.

Institutional Review Board Statement: Not applicable.

Informed Consent Statement: Not applicable.

Data Availability Statement: Not applicable.

Acknowledgments: M.B.-G. thanks PAIDI2020 research grant (DOC_00272 Junta de Andalucía, Spain) and R.M.P.C. thanks University of Malaga under Plan Propio de Investigación for financial support.

Conflicts of Interest: The authors declare no conflict of interest.

References

1. Shivhare, A.; Kumara, A.; Srivastava, R. Metal phosphate catalysts to upgrade ligno-cellulose biomass into value-added chemicals and biofuels. *Green Chem.* **2021**, *23*, 3818–3841. [[CrossRef](#)]
2. Zhao, H.; Yuan, Z.-Y. Insights into Transition Metal Phosphate Materials for Efficient Electrocatalysis. *ChemCatChem* **2020**, *12*, 3797–3810. [[CrossRef](#)]
3. Chen, L.; Zhao, Y.; Yang, J.; Liu, D.; Wei, X.; Wang, X.; Zheng, Y. New Versatile Synthetic Route for the Preparation of Metal Phosphate Decorated Hydrogen Evolution Photocatalysts. *Inorg. Chem.* **2020**, *59*, 1566–1575. [[CrossRef](#)]
4. Goñi-Urtiaga, A.; Presvytes, D.; Scott, K. Solid acids as electrolyte materials for proton exchange membrane (PEM) electrolysis: Review. *Int. J. Hydrog. Energy* **2012**, *37*, 3358–3372. [[CrossRef](#)]
5. Paschos, O.; Kunze, J.; Stimming, U.; Maglia, F. A review on phosphate based, solid state, protonic conductors for intermediate temperature fuel cells. *J. Phys. Condens. Matter* **2011**, *23*, 234110. [[CrossRef](#)]
6. Haile, S.M.; Chisholm, C.R.I.; Sasaki, K.; Boysen, D.A.; Uda, T. Solid acid proton conductors: From laboratory curiosities to fuel cell electrolytes. *Faraday Discuss.* **2007**, *134*, 17–39. [[CrossRef](#)] [[PubMed](#)]
7. Cheng, Q.; Zhao, X.; Yang, G.; Mao, L.; Liao, F.; Chen, F.; He, P.; Pan, D.; Chen, S. Recent advances of metal phosphates-based electrodes for high-performance metal ion batteries. *Energy Storage Mater.* **2021**, *41*, 842–882. [[CrossRef](#)]
8. Habraken, W.; Habibovic, P.; Epple, M.; Bohner, M. Calcium phosphates in biomedical applications: Materials for the future? *Mater. Today* **2015**, *19*, 69–87. [[CrossRef](#)]
9. Mohammad, N.; Mohamad, A.B.; Kadhum, A.A.H.; Loh, K.S. A review on synthesis and characterization of solid acid materials for fuel cell applications. *J. Power Sources* **2016**, *322*, 77–92. [[CrossRef](#)]
10. Pica, M.; Donnadio, A.; Casciola, M. From microcrystalline to nanosized α -zirconium phosphate: Synthetic approaches and applications of an old material with a bright future. *Coord. Chem. Rev.* **2018**, *374*, 218–235. [[CrossRef](#)]

11. Wong, N.E.; Ramaswamy, P.; Lee, A.S.; Gelfand, B.S.; Bladec, K.J.; Taylor, J.M.; Spasyuk, D.M.; Shimizu, G.K.H. Tuning Intrinsic and Extrinsic Proton Conduction in Metal–Organic Frameworks by the Lanthanide Contraction. *J. Am. Chem. Soc.* **2017**, *139*, 14676–14683. [[CrossRef](#)] [[PubMed](#)]
12. Horike, S.; Umeyama, D.; Inukai, M.; Itakura, T.; Kitagawa, S. Coordination-network-based ionic plastic crystal for anhydrous proton conductivity. *J. Am. Chem. Soc.* **2012**, *134*, 7612–7615. [[CrossRef](#)] [[PubMed](#)]
13. Zhang, K.-M.; Lou, Y.-L.; He, F.-Y.; Duan, H.-B.; Huang, X.-Q.; Fan, Y.; Zhao, H.-R. The water-mediated proton conductivity of a 1D open framework inorganic-organic hybrid iron phosphate and its composite membranes. *Inorg. Chem. Commun.* **2021**, *134*, 109032. [[CrossRef](#)]
14. Yu, J.-W.; Yu, H.-J.; Ren, Q.; Zhang, J.; Zou, Y.; Luo, H.-B.; Wang, L.; Ren, X.-M. Humidity-sensitive irreversible phase transformation of open-framework zinc phosphate and its water-assisted high proton conduction properties. *Dalton Trans.* **2021**, *50*, 8070–8075. [[CrossRef](#)] [[PubMed](#)]
15. Su, X.; Yao, Z.; Ye, Y.; Zeng, H.; Xu, G.; Wu, L.; Ma, X.; Chen, Q.-H.; Wang, L.; Zhang, Z.; et al. 40-Fold Enhanced Intrinsic Proton Conductivity in Coordination Polymers with the Same Proton-Conducting Pathway by Tuning Metal Cation Nodes. *Inorg. Chem.* **2016**, *55*, 983–986. [[CrossRef](#)]
16. Shi, J.; Wang, K.; Li, J.; Zeng, H.; Zhang, Q.; Lin, Z. Exploration of new water stable proton-conducting materials in an amino acid-templated metal phosphate system. *Dalton Trans.* **2018**, *47*, 654–658. [[CrossRef](#)]
17. Zhang, K.-M.; He, F.-Y.; Duan, H.-B.; Zhao, H.-R. An alkali metal ion-exchanged metal-phosphate $(C_2H_{10}N_2)_xNa_{1-x}[Mn_2(PO_4)_2]$ with high proton conductivity of $10^{-2} S \cdot cm^{-1}$. *Inorg. Chem.* **2019**, *58*, 6639–6646. [[CrossRef](#)]
18. Zhang, K.-M.; Jia, Y.; Gu, Y.; He, F.-Y.; Zhao, H.-R. A facile and efficient method to improve the proton conductivity of open framework metal phosphates under aqueous condition. *Inorg. Chem. Commun.* **2020**, *120*, 108128. [[CrossRef](#)]
19. Umeyama, D.; Horike, S.; Inukai, M.; Kitagawa, S. Integration of Intrinsic Proton Conduction and Guest-Accessible Nanospace into a Coordination Polymer. *J. Am. Chem. Soc.* **2013**, *135*, 11345–11350. [[CrossRef](#)]
20. Baranov, A.I.; Khiznichenko, V.P.; Sandler, V.A.; Shuvalov, L.A. Frequency dielectric dispersion in the ferroelectric and superionic phases of CsH_2PO_4 . *Ferroelectrics* **1988**, *81*, 183–186. [[CrossRef](#)]
21. Colomban, P. Chemistry of Solid-State Materials. In *Proton Conductors: Solid, Membranes and Gels-Materials and Devices*; Cambridge University Press: Cambridge, UK, 1992.
22. Fragua, D.M.; Castillo, J.; Castillo, R.; Vargas, R.A. New amorphous phase $KnH_2P_nO_{3n+1}$ ($n > 1$) in KH_2PO_4 . *Rev. Latin Am. Metal. Mat.* **2009**, *2*, 491–497.
23. Skou, E.; Andersen, I.G.K.; Simonsen, K.E.; Andersen, E.K. Is $UO_2HPO_4 \cdot 4H_2O$ a proton conductor? *Solid State Ion.* **1983**, *9*, 1041–1047. [[CrossRef](#)]
24. Cabeza, A.; Martinez, M.; Benavente, J.; Bruque, S. Current rectification by $H_3OUO_2PO_4 \cdot 3H_2O$ (HUP) thin films in electrolyte media. *Solid State Ion.* **1992**, *51*, 127–131. [[CrossRef](#)]
25. Barboux, P.; Morineau, R.; Livage, J. Protonic conductivity in hydrates. *Solid State Ion.* **1988**, *27*, 221–225. [[CrossRef](#)]
26. Barboux, P.; Livage, J. Ionic conductivity in fibrous $Ce(HPO_4)_2 \cdot (3+x)H_2O$. *Solid State Ion.* **1989**, *34*, 47–52. [[CrossRef](#)]
27. Li, J.; Yi, M.; Zhang, L.; You, Z.; Liu, X.; Li, B. Energy related ion transports in coordination polymers. *Nano Select.* **2021**, 1–19. [[CrossRef](#)]
28. Steele, B.C.H.; Heinzl, A. Materials for fuel-cell technologies. *Nature* **2001**, *414*, 245–260. [[CrossRef](#)]
29. Wei, J. Proton-Conducting Materials Used as Polymer Electrolyte Membranes in Fuel Cells (ch 9). In *Polymer-Based Multifunctional Nanocomposites and Their Applications*; Song, K., Liu, C., Guo, J.Z., Eds.; Elsevier: Amsterdam, The Netherlands, 2019; Chapter 9; pp. 345–352.
30. Sazali, N.; Salleh, W.N.W.; Jamaludin, A.S.; Razali, M.N.M. New Perspectives on Fuel Cell Technology: A Brief Review. *Membranes* **2020**, *10*, 99. [[CrossRef](#)] [[PubMed](#)]
31. Dupuis, A.-C. Proton exchange membranes for fuel cells operated at medium temperatures: Materials and experimental techniques. *Prog. Mater. Sci.* **2011**, *56*, 289–327. [[CrossRef](#)]
32. Peighambardoust, S.J.; Rowshanzamir, S.; Amjadi, M. Review of the proton exchange membranes for fuel cell applications. *Int. J. Hydrog. Energy* **2010**, *35*, 9349–9384. [[CrossRef](#)]
33. Mauritz, K.A.; Moore, R.B. State of understanding of Nafion. *Chem. Rev.* **2004**, *104*, 4535–4585. [[CrossRef](#)] [[PubMed](#)]
34. Hickner, M.A.; Ghassemi, H.; Kim, Y.S.; Einsla, B.R.; McGrath, J.E. Alternative polymer systems for proton exchange membranes (PEMs). *Chem. Rev.* **2004**, *104*, 4587–4612. [[CrossRef](#)] [[PubMed](#)]
35. Han, X.; Xie, Y.; Liu, D.; Chen, Z.; Zhang, H.; Pang, J.; Jiang, Z. Synthesis and properties of novel poly(arylene ether)s with densely sulfonated units based on carbazole derivative. *J. Membr. Sci.* **2019**, *589*, 117230. [[CrossRef](#)]
36. Kuzmenko, M.; Poryadchenko, N. Perspective materials for application in fuel-cell technologies. In *Fuel Cell Technologies: State and Perspectives*; Sammes, N., Ed.; Springer: Dordrecht, The Netherlands, 2005; pp. 253–258.
37. Lee, K.-S.; Maurya, S.; Kim, Y.S.; Kreller, C.R.; Wilson, M.S.; Larsen, D.; Elangovan, S.E.; Mukundan, R. Intermediate temperature fuel cells via an ion-pair coordinated polymer electrolyte. *Energy Env. Sci.* **2018**, *11*, 979–987. [[CrossRef](#)]
38. Norby, T. Solid-state protonic conductors: Principles, properties, progress and prospects. *Solid State Ion.* **1999**, *125*, 1–11. [[CrossRef](#)]
39. Li, Q.; He, R.; Jensen, J.O.; Bjerrum, N.J. Approaches and Recent Development of Polymer Electrolyte Membranes for Fuel Cells Operating above 100 °C. *Chem. Mater.* **2003**, *15*, 4896–4915. [[CrossRef](#)]

40. Loreti, G.; Facci, A.L.; Ubertini, S. High-Efficiency Combined Heat and Power through a High-Temperature Polymer Electrolyte Membrane Fuel Cell and Gas Turbine Hybrid System. *Sustainability* **2021**, *13*, 12515. [[CrossRef](#)]
41. Boysen, D.A.; Uda, T.; Chisholm, C.R.I.; Haile, S.M. High-Performance Solid Acid Fuel Cells Through Humidity Stabilization. *Science* **2004**, *303*, 68–70. [[CrossRef](#)]
42. Zhang, J.; Aili, D.; Lu, S.; Li, Q.; Jiang, S.P. Advancement toward Polymer Electrolyte Membrane Fuel Cells at Elevated Temperatures. *AAAS Res.* **2020**, *2020*, 9089405. [[CrossRef](#)]
43. Clearfield, A.; Smith, S.D. The crystal structure of zirconium phosphate and the mechanism of its ion exchange behavior. *J. Colloid Interface Sci.* **1968**, *28*, 325–330. [[CrossRef](#)]
44. Clearfield, A.; Smith, G.D. Crystallography and structure of alpha-zirconium bis(monohydrogen orthophosphate) monohydrate. *Inorg. Chem.* **1969**, *8*, 431–436. [[CrossRef](#)]
45. Troup, J.M.; Clearfield, A. Mechanism of ion exchange in zirconium phosphates. 20. Refinement of the crystal structure of alpha-zirconium phosphate. *Inorg. Chem.* **1977**, *16*, 3311–3314. [[CrossRef](#)]
46. Casciola, M. From layered zirconium phosphates and phosphonates to nanofillers for ionomeric membranes. *Solid State Ion.* **2019**, *336*, 1–10. [[CrossRef](#)]
47. Ogawa, T.; Ushiyam, H.; Lee, J.-M.; Yamaguchi, T.; Yamashita, K. Theoretical Studies on Proton Transfer among a High Density of Acid Groups: Surface of Zirconium Phosphate with Adsorbed Water Molecules. *J. Phys. Chem. C* **2011**, *115*, 5599–5606. [[CrossRef](#)]
48. Alberti, G.; Casciola, M.; Costantino, U. Inorganic ion-exchange pellicles obtained by delamination of alpha-zirconium phosphate crystals. *J. Colloid Interface Sci.* **1985**, *107*, 256–263. [[CrossRef](#)]
49. Alberti, G.; Casciola, M.; Costantino, U.; Leonardi, M. AC conductivity of anhydrous pellicular zirconium phosphate in hydrogen form. *Solid State Ion.* **1984**, *14*, 289–295. [[CrossRef](#)]
50. Casciola, M.; Costantino, U.; D'Amico, S. Protonic conduction of intercalation compounds of alpha-zirconium phosphate with propylamine. *Solid State Ion.* **1986**, *22*, 127–133. [[CrossRef](#)]
51. Alberti, G.; Casciola, M.; Cavalaglio, S.; Vivani, R. Proton conductivity of mesoporous zirconium phosphate pyrophosphate. *Solid State Ion.* **1999**, *125*, 91–97. [[CrossRef](#)]
52. Alberti, G.; Casciola, M.; Donnadio, A.; Piaggio, P.; Pica, M.; Sisani, M. Preparation and characterisation of alpha-layered zirconium phosphate sulfophenylphosphonates with variable concentration of sulfonic groups. *Solid State Ion.* **2005**, *176*, 2893–2898. [[CrossRef](#)]
53. Gui, D.; Zheng, T.; Xie, J.; Cai, Y.; Wang, Y.; Chen, L.; Diwu, J.; Chai, Z.; Wang, S. Significantly dense two-dimensional hydrogen-bond network in a layered zirconium phosphate leading to high proton conductivities in both water-assisted low-temperature and anhydrous intermediate-temperature regions. *Inorg. Chem.* **2016**, *55*, 12508–12511. [[CrossRef](#)]
54. Yu, J.-W.; Yu, H.-J.; Yao, Z.-Y.; Li, Z.-H.; Ren, Q.; Luo, H.-B.; Zou, Y.; Wang, L.; Ren, X.-M. A water-stable open-framework zirconium(IV) phosphate and its water-assisted high proton conductivity. *CrystEngComm* **2021**, *23*, 6093–6097. [[CrossRef](#)]
55. Gui, D.; Dai, X.; Tao, Z.; Zheng, T.; Wang, X.; Silver, M.A.; Shu, J.; Chen, L.; Wang, Y.; Zhang, T.; et al. Unique proton transportation pathway in a robust inorganic coordination polymer leading to intrinsically high and sustainable anhydrous proton conductivity. *J. Am. Chem. Soc.* **2018**, *140*, 6146–6155. [[CrossRef](#)]
56. Kusoglu, A.; Weber, A.Z. New Insights into Perfluorinated Sulfonic-Acid Ionomers. *Chem. Rev.* **2017**, *117*, 987–1104. [[CrossRef](#)]
57. Alberti, G.; Casciola, M.; Capitani, D.; Donnadio, A.; Narducci, R.; Pica, M.; Sganappa, M. Novel Nafion-zirconium phosphate nanocomposite membranes with enhanced stability of proton conductivity at medium temperature and high relative humidity. *Electrochim. Acta* **2007**, *52*, 8125–8132. [[CrossRef](#)]
58. Grot, W.G.; Rajendran, G.; Hendrickson, J.S. Membranes Containing Inorganic Fillers and Membranes and Electrode Assemblies and Electrochemical Cells Employing Same. International Publication No. WO 96/2975, 26 September 1996.
59. Alberti, G.; Casciola, M.; Pica, M.; Tarpanelli, T.; Sganappa, M. New Preparation Methods for Composite Membranes for Medium Temperature Fuel Cells Based on Precursor Solutions of Insoluble Inorganic Compounds. *Fuel Cells* **2005**, *5*, 366–374. [[CrossRef](#)]
60. Casciola, M.; Bagnasco, G.; Donnadio, A.; Micoli, L.; Pica, M.; Sganappa, M.; Turco, M. Conductivity and Methanol Permeability of Nafion-Zirconium Phosphate Composite Membranes Containing High Aspect Ratio Filler Particles. *Fuel Cells* **2009**, *9*, 394–400. [[CrossRef](#)]
61. Arbizzani, C.; Donnadio, A.; Pica, M.; Sganappa, M.; Varzi, A.; Casciola, M.; Mastragostino, M. Methanol permeability and performance of Nafion-zirconium phosphate composite membranes in active and passive direct methanol fuel cells. *J. Power Sources* **2010**, *195*, 7751–7756. [[CrossRef](#)]
62. Pica, M.; Donnadio, A.; Casciola, M.; Cojocar, P.; Merlo, L. Short side chain perfluorosulfonic acid membranes and their composites with nanosized zirconium phosphate: Hydration, mechanical properties and proton conductivity. *J. Mater. Chem.* **2012**, *22*, 24902–24908. [[CrossRef](#)]
63. Pica, M.; Donnadio, A.; Capitani, D.; Vivani, R.; Troni, E.; Casciola, M. Advances in the Chemistry of Nanosized Zirconium Phosphates: A New Mild and Quick Route to the Synthesis of Nanocrystals. *Inorg. Chem.* **2011**, *50*, 11623–11630. [[CrossRef](#)] [[PubMed](#)]
64. Bauer, F.; Willert-Porada, M. Comparison between Nafion and a Nafion zirconium phosphate nanocomposite in fuel cell applications. *Fuel Cells* **2006**, *6*, 261–269. [[CrossRef](#)]

65. Casciola, M.; Cojocar, P.; Donnadio, A.; Giancola, S.; Merlo, L.; Nedellec, Y.; Pica, M.; Subianto, S. Zirconium phosphate reinforced short side chain perfluorosulfonic acid membranes for medium temperature proton exchange membrane fuel cell application. *J. Power Sources* **2014**, *262*, 407–413. [[CrossRef](#)]
66. Yang, C.; Srinivasan, S.; Aricò, A.S.; Creti, P.; Baglio, V.; Antonucci, V. Composition Nafion/zirconium phosphate membranes for direct methanol fuel cell operation at high temperature. *Electrochim. Solid-State Lett.* **2001**, *4*, A31–A34. [[CrossRef](#)]
67. Yang, C.; Costamagna, P.; Srinivasan, S.; Benziger, J.; Bocarsly, A.B. Approaches and technical challenges to high temperature operation of proton exchange membrane fuel cells. *J. Power Sources* **2001**, *103*, 1–9. [[CrossRef](#)]
68. Costamagna, P.; Yang, C.; Bocarsly, A.B.; Srinivasan, S. Nafion (R) 115/zirconium phosphate composite membranes for operation of PEMFCs above 100 °C. *Electrochim. Acta* **2002**, *47*, 1023–1033. [[CrossRef](#)]
69. Yang, C.; Srinivasan, S.; Bocarsly, A.B.; Tulyani, S.; Benziger, J.B. A comparison of physical properties and fuel cell performance of Nafion and zirconium phosphate/Nafion composite membranes. *J. Membr. Sci.* **2004**, *237*, 145–161. [[CrossRef](#)]
70. Lee, H.-K.; Kim, J.-I.; Park, J.-H.; Lee, T.-H. A study on self-humidifying PEMFC using Pt-ZrP-Nafion composite membrane. *Electrochim. Acta* **2004**, *50*, 761–768. [[CrossRef](#)]
71. Escorihuela, J.; Narducci, R.; Compañ, V.; Costantino, F. Proton Conductivity of Composite Polyelectrolyte Membranes with Metal-Organic Frameworks for Fuel Cell Applications. *Adv. Mater. Interfaces* **2019**, *6*, 1801146. [[CrossRef](#)]
72. Liu, K.L.; Lee, H.C.; Wang, B.Y.; Lue, S.J.; Lu, C.Y.; Tsai, L.D.; Fang, J.; Chao, C.Y. Sulfonated poly(styrene-block-(ethylene-ran-butylene)-block-styrene (SSEBS)-zirconium phosphate) (ZrP) composite membranes for direct methanol fuel cells. *J. Membr. Sci.* **2015**, *495*, 110–120. [[CrossRef](#)]
73. Hu, H.; Ding, F.; Ding, H.; Liu, J.; Xiao, M.; Meng, Y.; Sun, L. Sulfonated poly(flourenyl ether ketone)/Sulfonated α -zirconium phosphate Nanocomposite membranes for proton exchange membrane fuel cells. *Adv. Compos. Hybrid Mater.* **2020**, *3*, 498–507. [[CrossRef](#)]
74. Pandey, J.; Seepana, M.M.; Shukla, A. Zirconium phosphate based proton conducting membrane for DMFC application. *Int. J. Hydrog.* **2015**, *40*, 9410–9421. [[CrossRef](#)]
75. He, R.; Li, Q.; Xiao, G.; Bjerrum, N.J. Proton conductivity of phosphoric acid doped polybenzimidazole and its composites with inorganic proton conductors. *J. Membr. Sci.* **2003**, *226*, 169–184. [[CrossRef](#)]
76. Gouda, M.H.; Tamer, T.M.; Konsowa, A.H.; Farag, H.A.; Mohy Eldin, M.S. Organic-Inorganic Novel Green Cation Exchange Membranes for Direct Methanol Fuel Cells. *Energies* **2021**, *14*, 4686. [[CrossRef](#)]
77. Alberti, G.; Cardini-Galli, P.; Costantino, U.; Torracca, E. Crystalline insoluble salts of polybasic metals—I Ion-exchange properties of crystalline titanium phosphate. *J. Inorg. Nucl. Chem.* **1967**, *29*, 571–578. [[CrossRef](#)]
78. Christensen, A.N.; Anderson, E.K.; Andersen, I.G.; Alberti, G.; Nielsen, M.; Lehmann, E.K. X-Ray Powder diffraction study of layer compounds. The crystal structure of α -Ti (HPO₄)₂·2H₂O and a proposed structure for γ -Ti (H₂PO₄)(PO₄)₂·2H₂O. *Acta Chem. Scand.* **1990**, *44*, 865–872. [[CrossRef](#)]
79. Li, Y.J.; Whittingham, M.S. Hydrothermal synthesis of new metastable phases: Preparation and intercalation of a new layered titanium phosphate. *Solid State Ion.* **1993**, *63*, 391–395. [[CrossRef](#)]
80. Kőrösi, L.; Papp, S.; Dékány, I. A layered titanium phosphate Ti₂O₃(H₂PO₄)₂·2H₂O with rectangular morphology: Synthesis, structure, and cysteamine intercalation. *Chem. Mater.* **2010**, *22*, 4356–4363. [[CrossRef](#)]
81. Ekambaram, S.; Serre, C.; Férey, G.; Sevov, S.C. Hydrothermal synthesis and characterization of an ethylenediamine-templated mixed-valence titanium phosphate. *Chem. Mater.* **2000**, *12*, 444–449. [[CrossRef](#)]
82. Krogh Andersen, A.M.; Norby, P.; Hanson, J.C.; Vogt, T. Preparation and characterization of a new 3-dimensional zirconium hydrogen phosphate, τ -Zr(HPO₄)₂. Determination of the complete crystal structure combining synchrotron X-ray single-crystal diffraction and neutron powder diffraction. *Inorg. Chem.* **1998**, *37*, 876–881. [[CrossRef](#)]
83. Mileo, P.G.M.; Kundu, T.; Semino, R.; Benoit, V.; Steunou, N.; Llewellyn, P.L.; Serre, C.; Maurin, G.; Devautour-Vinot, S. Highly Efficient Proton Conduction in a Three-Dimensional Titanium Hydrogen Phosphate. *Chem. Mater.* **2017**, *29*, 7263–7271. [[CrossRef](#)]
84. Bortun, A.I.; Khainakov, S.A.; Bortun, L.N.; Poojary, D.M.; Rodriguez, J.; Jose, R.; Garcia, J.R.; Clearfield, A. Synthesis and characterization of two novel fibrous titanium phosphates Ti₂O(PO₄)₂·2H₂O. *Chem. Mater.* **1997**, *9*, 1805–1811. [[CrossRef](#)]
85. Salvadó, M.A.; Pertierra, P.; García-Granda, S.; García, J.R.; Fernández-Díaz, M.T.; Dooryhee, E. Crystal structure, including H-atom positions, of Ti₂O(PO₄)₂·(H₂O)₂ determined from synchrotron X-ray and neutron powder data. *Eur. J. Solid State Inorg. Chem.* **1997**, *34*, 1237–1247. [[CrossRef](#)]
86. Babaryk, A.A.; Adawy, A.; García, I.; Trobajo, C.; Amghouz, Z.; Colodrero, A.R.M.P.; Olivera-Pastor, P.; Bazaga-García, M.; dos Santos-Gómez, L. Structural and proton conductivity studies of fibrous π -Ti₂O(PO₄)₂·2H₂O: Application in chitosan-based composite membranes. *Dalton Trans.* **2021**, *50*, 7667–7677. [[CrossRef](#)] [[PubMed](#)]
87. Bruque, S.; Aranda, M.A.G.; Losilla, E.R.; Olivera-Pastor, P.; Maireles-Torres, P. Synthesis optimization and crystal structures of layered metal(IV) hydrogen phosphates, α -M(HPO₄)₂·nH₂O (M = Ti, Sn, Pb). *Inorg. Chem.* **1995**, *34*, 893–899. [[CrossRef](#)]
88. Huang, W.; Komarneni, S.; Noh, Y.D.; Ma, J.; Chen, K.; Xue, D.; Xue, X.; Jiang, B. Novel inorganic tin phosphate gel: Multifunctional material. *Chem. Commun.* **2018**, *54*, 2682–2685. [[CrossRef](#)] [[PubMed](#)]
89. Ansari, Y.; Telpriere, G.; Tucker, C.; Angell, A. A novel, easily synthesized, anhydrous derivative of phosphoric acid for use in electrolyte with phosphoric acid-based fuel cells. *J. Power Sources* **2013**, *237*, 47–51. [[CrossRef](#)]

90. Moshareva, M.A.; Novikova, S.A.; Yaroslavtsev, A.B. Synthesis and ionic conductivity of $(\text{NH}_4)_{1-x} \text{H}_x \text{Hf}_2(\text{PO}_4)_3$ ($x = 0-1$) NASICON-type materials. *Inorg. Mater.* **2016**, *52*, 1283–1290. [[CrossRef](#)]
91. Clearfield, A. Structural concepts in inorganic proton conductors. *Solid State Ion.* **1991**, *46*, 34–43. [[CrossRef](#)]
92. Clearfield, A.; Roberts, B.D.; Subramanian, M.A. Preparation of $(\text{NH}_4)\text{Zr}_2(\text{PO}_4)_3$ and $\text{HZr}_2(\text{PO}_4)_3$. *Mater. Res. Bull.* **1984**, *19*, 219–226. [[CrossRef](#)]
93. Komorowski, P.G.; Agryropoulos, S.A.A.; Canaday, J.D.; Kuriakose, A.K.; Wheat, T.A.; Ahmad, A.; Gulens, J. The study of hydronium NASICON conductivity with deuterium. *Solid State Ion.* **1992**, *50*, 253–258. [[CrossRef](#)]
94. Stenina, I.A.; Kisilitsyn, M.N.; Ghuravlev, N.A.; Yaroslavtsev, A.B. Phase transitions and ionic mobility in hydrogen zirconium phosphates with the NASICON structure, $\text{H}_{1 \pm x} \text{Zr}_{2-x} \text{M}_x(\text{PO}_4)_3 \cdot \text{H}_2\text{O}$, $\text{M} = \text{Nb}$, Y . *Mater. Res. Bull.* **2008**, *43*, 377–383. [[CrossRef](#)]
95. Stenina, A.; Pinus, I.Y.; Rebrov, A.I.; Yaroslavtsev, A.B. Lithium and hydrogen ions transport in materials with NASICON structure. *Solid State Ion.* **2004**, *175*, 445–449. [[CrossRef](#)]
96. Stenina, I.A.; Zhizhin, M.G.; Lazoryak, B.I.; Yaroslavtsev, A.B. Phase transitions, structure and ion conductivity of zirconium hydrogen phosphates, $\text{H}_{1 \pm x} \text{Zr}_{2-x} \text{M}_x(\text{PO}_4)_3 \cdot \text{H}_2\text{O}$ ($\text{M} = \text{Nb}$, Y). *Mater. Res. Bull.* **2009**, *44*, 1608–1612. [[CrossRef](#)]
97. Mieritz, D.; Davidowski, S.K.; Seo, D. Accessing alkali-free NASICON-type compounds through mixed oxoanion sol-gel chemistry: Hydrogen titanium phosphate sulfate, $\text{H}_{1-x} \text{Ti}_2(\text{PO}_4)_{3-x}(\text{SO}_4)_x$ ($x=0.5-1$). *J. Solid State Chem.* **2016**, *242*, 116–125. [[CrossRef](#)]
98. Sato, Y.; Shen, Y.; Nishida, M.; Kanematsu, W.; Hibino, T. Proton Conduction in Non-Doped and Acceptor-Doped Metal Pyrophosphate (MP_2O_7) Composite Ceramics at Intermediate Temperatures. *J. Mater. Chem.* **2012**, *22*, 3973–3981. [[CrossRef](#)]
99. Singh, B.; Kima, J.-H.; Park, J.-Y.; Song, S.-J. Dense composite electrolytes of Gd^{3+} -doped cerium phosphates for low-temperature proton-conducting ceramic-electrolyte fuel cells. *Ceram. Inter.* **2015**, *41*, 4814–4821. [[CrossRef](#)]
100. Nagao, M.; Kamiya, T.; Heo, P.; Tomita, A.; Hibino, T.; Sano, M. Proton conduction in In^{3+} -doped SnP_2O_7 at intermediate temperatures. *J. Electrochem. Soc.* **2006**, *153*, 1604–1609. [[CrossRef](#)]
101. Nagao, M.; Takeuchi, A.; Heo, P.; Hibino, T.; Sano, M.; Tomita, A. A proton-conducting In^{3+} -doped SnP_2O_7 electrolyte for intermediate-temperature fuel cells. *Electrochem. Solid-State Lett.* **2006**, *9*, A105. [[CrossRef](#)]
102. Jin, Y.; Fujiwara, K.; Hibino, T. High temperature, low humidity proton exchange membrane based on an inorganic-organic hybrid structure. *Electrochem. Solid-State Lett.* **2010**, *13*, B8. [[CrossRef](#)]
103. Jin, Y.; Shen, Y.; Hibino, T. Proton conduction in metal pyrophosphates (MP_2O_7) at intermediate temperatures. *J. Mater. Chem.* **2010**, *20*, 6214–6217. [[CrossRef](#)]
104. Chen, X.; Wang, C.; Payzant, E.; Xia, C.; Chu, D. An oxide ion and proton co-ion conducting $\text{Sn}_0.9\text{In}_0.1\text{P}_2\text{O}_7$ electrolyte for intermediate-temperature fuel cells. *J. Electrochem. Soc.* **2008**, *155*, B1264. [[CrossRef](#)]
105. Kreller, C.R.; Pham, H.H.; Wilson, M.S.; Mukundan, R.; Henson, N.; Sykora, M.; Hartl, M.; Daemen, L.; Garzon, F.H. Intragranular phase proton conduction in crystalline $\text{Sn}_{1-x}\text{In}_x\text{P}_2\text{O}_7$ ($x = 0$ and 0.1). *J. Phys. Chem. C* **2017**, *121*, 23896–23905. [[CrossRef](#)]
106. Kreller, C.R.; Wilson, M.S.; Mukundan, R.; Brosha, E.L.; Garzon, F.H. Stability and conductivity of In^{3+} -doped SnP_2O_7 with varying phosphorous to metal ratios. *ECS Electrochem. Lett.* **2013**, *2*, F61–F63. [[CrossRef](#)]
107. Foran, G.Y.; Goward, G.R. Site-Specific Proton Dynamics in Indium-Doped Tin Pyrophosphate. *J. Phys. Chem. C* **2020**, *124*, 28407–28416. [[CrossRef](#)]
108. Scott, K.; Xu, C.; Wu, X. Intermediate temperature proton-conducting membrane electrolytes for fuel cells. *Wiley Interdiscip. Rev. Energy Environ.* **2014**, *3*, 24–41. [[CrossRef](#)]
109. Anfimova, T.; Lie-Andersena, T.; Pristed Jensen, E.; Brorson Prag, C.; Nielsen, U.G.; Sørensen, D.R.; Skou, E.M.; Christensen, E.; Bjerrum, N.J.; Li, Q. The effect of preparation method on the proton conductivity of indium doped tin pyrophosphates. *Solid State Ion.* **2015**, *278*, 209–216. [[CrossRef](#)]
110. Li, W.; Bose, A.B.; Rusakova, I.A. An approach for restoring the proton conductivity of sintered tin pyrophosphate membranes for intermediate temperature fuel cells. *J. Power Sources* **2016**, *307*, 146–151. [[CrossRef](#)]
111. Ramaiyan, K.P.; Herrera, S.; Workman, M.J.; Semelsberger, T.A.; Atanasov, V.; Kerres, J.; Sandip Maurya, S.; Kim, Y.S.; Kreller, C.R.; Mukundan, R. Role of phosphate source in improving the proton conductivity of tin pyrophosphate and its composite electrolytes. *J. Mater. Chem. A* **2020**, *8*, 16345–16354. [[CrossRef](#)]
112. Wu, X.; Mamlouk, M.; Scott, K. A $\text{PBI-Sb}_{0.2}\text{Sn}_{0.8}\text{P}_2\text{O}_7\text{-H}_3\text{PO}_4$ Composite Membrane. *Fuel Cells* **2011**, *11*, 620–625. [[CrossRef](#)]
113. Jin, Y.C.; Nishida, M.; Kanematsu, W.; Hibino, T. An H_3PO_4 -doped polybenzimidazole/ $\text{Sn}_{0.95}\text{Al}_{0.05}\text{P}_2\text{O}_7$ composite membrane for high-temperature proton exchange membrane fuel cells. *J. Power Sources* **2011**, *196*, 6042–6047. [[CrossRef](#)]
114. Huang, M.; Huang, X.; Deng, Y.; Fei, M.; Xu, C.; Cheng, J. Graphite oxide-incorporated SnP_2O_7 solid composite electrolyte for high-temperature proton exchange membrane fuel cells. *Int. J. Hydrog. Energy* **2017**, *42*, 1113–1119. [[CrossRef](#)]
115. Le, M.-V.; Tsai, D.-S.; Yang, C.-Y.; Chung, W.-H.; Lee, H.-Y. Proton conductors of cerium pyrophosphate for intermediate temperature fuel cell. *Electrochim. Acta* **2011**, *56*, 6654–6660. [[CrossRef](#)]
116. Hogarth, W.H.J.; Muir, S.S.; Whittaker, A.K.; Diniz da Costa, J.C.; Drennan, J.; Lu, G.Q. Proton conduction mechanism and the stability of sol-gel titanium phosphates. *Solid State Ion.* **2007**, *177*, 3389–3394. [[CrossRef](#)]
117. Alberti, G.; Costantino, U.; Casciola, M.; Ferroni, S.; Massinelli, L.; Staiti, P. Preparation, characterization and proton conductivity of titanium phosphate sulfophenylphosphonate. *Solid State Ion.* **2001**, *145*, 249–255. [[CrossRef](#)]
118. Zhang, L.; Liu, X.; Sun, X.; Jian, J.; Li, G.; Yuan, H. Proton conduction in organically templated 3D open-framework vanadium-nickel pyrophosphate. *Inorg. Chem.* **2019**, *58*, 4394–4398. [[CrossRef](#)] [[PubMed](#)]

119. Botez, C.E.; Tackett, R.J.; Hermosillo, J.D.; Zhang, J.; Zhao, Y.; Wang, L. High pressure synchrotron x-ray diffraction studies of superprotonic transitions in phosphate solid acids. *Solid State Ion.* **2012**, *213*, 58–62. [[CrossRef](#)]
120. Baranov, A.I. Crystals with disordered hydrogen-bond networks and superprotonic conductivity. Review. *Crystallogr. Rep.* **2003**, *48*, 1012–1037. [[CrossRef](#)]
121. Bagryantseva, I.N.; Gaydamaka, A.A.; Ponomareva, V.G. Intermediate temperature proton electrolytes based on cesium dihydrogen phosphate and Butyral polymer. *Ionics* **2020**, *26*, 1813–1818. [[CrossRef](#)]
122. Drefßler, C.; Sebastiani, D. Effect of anion reorientation on proton mobility in the solid acids family CsH_yXO_4 ($\text{X} = \text{S}, \text{P}, \text{Se}$, $y = 1, 2$) from ab initio molecular dynamics simulations. *Phys. Chem. Chem. Phys.* **2020**, *22*, 10738–10752. [[CrossRef](#)]
123. Taninouchi, Y.K.; Uda, T.; Awakura, Y.; Ikeda, A.; Haile, S.M. Dehydration behavior of the superprotonic conductor CsH_2PO_4 at moderate temperatures: 230 to 260 °C. *J. Mater. Chem.* **2007**, *17*, 3182–3189. [[CrossRef](#)]
124. Mathur, L.; Kim, I.-H.; Bhardwaj, A.; Singh, B.; Park, J.-Y.; Song, S.-J. Structural and electrical properties of novel phosphate based composite electrolyte for low-temperature fuel cells. *Composites Part B* **2020**, *202*, 108405. [[CrossRef](#)]
125. Otomo, J.; Tamaki, T.; Nishida, S.; Wang, S.; Ogura, M.; Kobayashi, T.; Wen, C.-J.; Nagamoto, H.; Takahashi, H. Effect of water vapor on proton conduction of cesium dihydrogen phosphate and application to intermediate temperature fuel cells. *J. Appl. Electrochem.* **2005**, *35*, 865–870. [[CrossRef](#)]
126. Uda, T.; Haile, S.M. Thin-membrane solid-acid fuel cell. *Electrochem. Solid State Lett.* **2005**, *8*, A245–A246. [[CrossRef](#)]
127. Navarrete, L.; Andrio, A.; Escolástico, S.; Moya, S.; Compañ, V.; Serra, J.M. Protonic Conduction of Partially-Substituted CsH_2PO_4 and the Applicability in Electrochemical Devices. *Membranes* **2019**, *9*, 49. [[CrossRef](#)]
128. Ponomareva, V.G.; Bagryantseva, I.N.; Gaydamaka, A.A. Study of the Phase Composition and Electrotransport Properties of the Systems Based on Mono- and Disubstituted Phosphates of Cesium and Rubidium. *Chem. Sustain. Dev.* **2019**, *27*, 238–245.
129. Martsinkevich, V.V.; Ponomareva, V.G. Double salts $\text{Cs}_{1-x}\text{M}_x\text{H}_2\text{PO}_4$ ($\text{M} = \text{Na}, \text{K}, \text{Rb}$) as proton conductors. *Solid State Ion.* **2012**, *225*, 236–240. [[CrossRef](#)]
130. Ponomareva, V.G.; Bagryantseva, I.N. Superprotonic CsH_2PO_4 - CsHSO_4 solid solutions. *Inorg. Mater.* **2012**, *48*, 187–194. [[CrossRef](#)]
131. Ponomareva, V.G.; Uvarov, N.F.; Lavrova, G.V.; Hairetdinov, E.F. Composite protonic solid electrolytes in the CsHSO_4 - SiO_2 system. *Solid State Ion.* **1996**, *90*, 161–166. [[CrossRef](#)]
132. Ponomareva, V.G.; Shutova, E.S.; Matvienko, A.A. Conductivity of Proton Electrolytes Based on Cesium Hydrogen Sulfate Phosphate. *Inorg. Mater.* **2004**, *40*, 721–728. [[CrossRef](#)]
133. Otomo, J.; Minagawa, N.; Wen, C.-J.; Eguchi, K.; Takahashi, H. Protonic conduction of CsH_2PO_4 and its composite with silica in dry and humid atmospheres. *Solid State Ion.* **2003**, *156*, 357–369. [[CrossRef](#)]
134. Ponomareva, V.G.; Shutova, E.S. High-temperature behavior of CsH_2PO_4 and CsH_2PO_4 - SiO_2 composites. *Solid State Ion.* **2007**, *178*, 729–734. [[CrossRef](#)]
135. Singh, D.; Singh, J.; Kumar, P.; Veer, D.; Kumar, D.; Katiyar, R.S.; Kumar, A.; Kumar, A. The Influence of TiO_2 on the Proton Conduction and Thermal Stability of CsH_2PO_4 Composite Electrolytes. *S. Afr. J. Chem. Eng.* **2021**, *37*, 227–236. [[CrossRef](#)]
136. Singh, D.; Kumar, P.; Singh, J.; Veer, D.; Kumar, A.; Katiyar, R.S. Structural, thermal and electrical properties of composites electrolytes $(1-x)\text{CsH}_2\text{PO}_4/x\text{ZrO}_2$ ($0 \leq x \leq 0.4$) for fuel cell with advanced electrode. *SN Appl. Sci.* **2021**, *3*, 46. [[CrossRef](#)]
137. Veer, D.; Kumar, P.; Singh, D.; Kumar, D.; Katiyar, R.S. A synergistic approach to achieving high conduction and stability of $\text{CsH}_2\text{PO}_4/\text{NaH}_2\text{PO}_4/\text{ZrO}_2$ composites for fuel cells. *Mater. Adv.* **2021**, *3*, 409–417. [[CrossRef](#)]
138. Aili, D.; Gao, Y.; Han, J.; Li, Q. Acid-base chemistry and proton conductivity of CsHSO_4 , CsH_2PO_4 and their mixtures with N-heterocycles. *Solid State Ion.* **2017**, *306*, 13–19. [[CrossRef](#)]
139. Bagryantseva, I.N.; Ponomareva, V.G.; Khusnutdinov, V.R. Intermediate temperature proton electrolytes based on cesium dihydrogen phosphate and poly(vinylidene fluoride-co-hexafluoropropylene). *J. Mater. Sci.* **2021**, *56*, 14196–14206. [[CrossRef](#)]
140. Ponomareva, V.G.; Bagryantseva, I.N.; Shutova, E.S. Hybrid systems based on nanodiamond and cesium dihydrogen phosphate. *Mater. Today* **2020**, *25*, 521–524. [[CrossRef](#)]
141. Ponomareva, V.G.; Bagryantseva, I.N. Effect of the excess protons on the electrotransport, structural and thermodynamic properties of CsH_2PO_4 . *Solid State Ion.* **2017**, *304*, 90–95. [[CrossRef](#)]
142. Ponomareva, V.G.; Lavrova, G.V. The influence of $\text{Cs}_2\text{HPO}_4 \cdot \text{H}_2\text{O}$ impurity on the proton conductivity and thermal properties of CsH_2PO_4 . *Solid State Ion.* **2019**, *329*, 90–94. [[CrossRef](#)]
143. Wang, M.; Luo, H.-B.; Liu, S.-X.; Zou, Y.; Tian, Z.-F.; Li, L.; Liu, J.-L.; Ren, X.-M. Water assisted high proton conductance in a highly thermally stable and superior water-stable open-framework cobalt phosphate. *Dalton Trans.* **2016**, *45*, 19466–19472. [[CrossRef](#)]
144. Umeyama, D.; Horike, S.; Inukai, M.; Itakura, T.; Kitagawa, S. Inherent Proton Conduction in a 2D Coordination Framework. *J. Am. Chem. Soc.* **2012**, *134*, 12780–12785. [[CrossRef](#)]
145. Inukai, M.; Horike, S.; Chen, W.; Umeyama, D.; Itakura, T.; Kitagawa, S. Template-directed proton conduction pathways in a coordination framework. *J. Mater. Chem. A* **2014**, *2*, 10404–10409. [[CrossRef](#)]
146. Zhao, H.-R.; Xue, C.; Li, C.-P.; Zhang, K.-M.; Luo, H.-B.; Liu, S.-X.; Ren, X.-M. A Two-Dimensional inorganic–organic hybrid solid of manganese(II) hydrogenophosphate showing high proton conductivity at room temperature. *Inorg. Chem.* **2016**, *55*, 8971–8975. [[CrossRef](#)]
147. Phang, W.J.; Lee, W.R.; Yoo, K.; Ryu, D.W.; Kim, B.S.; Hong, C.S. PH-dependent proton conducting behavior in a metal-organic framework material. *Angew. Chem. Int. Ed.* **2014**, *53*, 8383–8387. [[CrossRef](#)] [[PubMed](#)]

148. Nagarkar, S.S.; Unni, S.M.; Sharma, A.; Kurungot, S.; Ghosh, S.K. Two-in-one: Inherent anhydrous and water-assisted high proton conduction in a 3D metal-organic framework. *Angew. Chem. Int. Ed.* **2014**, *53*, 2638–2642. [[CrossRef](#)]
149. Nguyen, N.T.T.; Furukawa, H.; Gándara, F.; Trickett, C.A.; Jeong, H.M.; Cordova, K.E.; Yaghi, O.M. Three-dimensional metal-catecholate frameworks and their ultrahigh proton conductivity. *J. Am. Chem. Soc.* **2015**, *137*, 15394–15397. [[CrossRef](#)]
150. Horike, S.; Chen, W.; Itakura, T.; Inukai, M.; Umeyama, D.; Asakura, H.; Kitagawa, S. Order-to-disorder structural transformation of a coordination polymer and its influence on proton conduction. *Chem. Commun.* **2014**, *50*, 10241–10243. [[CrossRef](#)] [[PubMed](#)]
151. Ma, N.; Kosasang, S.; Yoshida, A.; Horike, S. Proton-conductive coordination polymer glass for solid-state anhydrous proton batteries. *Chem. Sci.* **2021**, *12*, 5818–5824. [[CrossRef](#)] [[PubMed](#)]
152. Matsuda, Y.; Yonemura, M.; Koga, H.; Pitteloud, C.; Nagao, M.; Hirayama, M.; Kanno, R. Synthesis, crystal structure, and ionic conductivity of tunnel structure phosphates, $\text{RbMg}_{1-x}\text{H}_{2x}(\text{PO}_3)_3\text{y}(\text{H}_2\text{O})$. *J. Mater. Chem. A* **2013**, *1*, 15544–15551. [[CrossRef](#)]
153. Antraptseva, N.M.; Solod, N.V.; Povshuk, V.A. Electrical conductivity of solid solution of Co(II)-Zn dihydrophosphate and its thermolysis products. *Funct. Mater.* **2015**, *22*, 322–326. [[CrossRef](#)]
154. Fan, D.; Tian, P.; Xu, S.T.; Wang, D.H.; Yang, Y.; Li, J.Z.; Wang, Q.Y.; Yang, M.; Liu, Z.M. SAPO-34 templated by dipropylamine and diisopropylamine: Synthesis and catalytic performance in the methanol to olefin (MTO) reaction. *New J. Chem.* **2016**, *40*, 4236–4244. [[CrossRef](#)]
155. Yu, Y.; Zhu, J.; Liu, J.; Yan, Y.; Song, X. Synthesis and characterization of two layered aluminophosphates $[\text{R-C}_8\text{H}_{12}\text{N}]_8[\text{H}_2\text{O}]_2 \cdot [\text{Al}_8\text{P}_{12}\text{O}_{48}\text{H}_4]$ and $[\text{S-C}_8\text{H}_{12}\text{N}]_8[\text{H}_2\text{O}]_2 \cdot [\text{Al}_8\text{P}_{12}\text{O}_{48}\text{H}_4]$ with a mirror symmetric feature and their proton conductivity. *Dalton Trans.* **2017**, *46*, 9157–9162. [[CrossRef](#)] [[PubMed](#)]
156. Park, S.H.; Choi, W.; Choi, H.J.; Hong, S.B. Organic-Free Synthesis of Silicoaluminophosphate Molecular Sieves. *Angew. Chem. Int. Ed.* **2018**, *57*, 9413–9418. [[CrossRef](#)] [[PubMed](#)]
157. Wang, Y.Y.; Sun, Y.J.; Mu, Y.; Zhang, C.Q.; Li, J.Y.; Yu, J.H. Organotemplate-free hydrothermal synthesis of an aluminophosphate molecular sieve with AEN zeotype topology and properties of its derivatives. *Chem. Commun.* **2014**, *50*, 15400–15403. [[CrossRef](#)] [[PubMed](#)]
158. Sun, Y.J.; Yan, Y.; Wang, Y.Y.; Li, Y.; Li, J.Y.; Yu, J.H. High proton conduction in a new alkali metal-templated open-framework aluminophosphate. *Chem. Commun.* **2015**, *51*, 9317–9319. [[CrossRef](#)]
159. Parise, J.B. Crystal Structures of Related Novel Aluminophosphate Frameworks: Aipo₄-21(py), Aipo₄-EN3 (en) and A Structural Model for Alpo₄-25. In *Studies in Surface Science and Catalysis*; Drzaj, S.H.B., Pejovnik, S., Eds.; Elsevier: Amsterdam, The Netherlands, 1985; Volume 24, pp. 271–278.
160. Parnham, E.R.; Morris, R.E. The ionothermal synthesis of cobalt aluminophosphate zeolite frameworks. *J. Am. Chem. Soc.* **2006**, *128*, 2204–2205. [[CrossRef](#)]
161. Wei, Y.; Tian, Z.; Gies, H.; Xu, R.; Ma, H.; Pei, R.; Zhang, W.; Xu, Y.; Wang, L.; Li, K.; et al. Ionothermal synthesis of an aluminophosphate molecular sieve with 20-ring pore openings. *Angew. Chem. Int. Ed.* **2010**, *49*, 5367–5370. [[CrossRef](#)]
162. Liu, L.; Yang, J.; Li, J.; Dong, J.; Šišak, D.; Luzzatto, M.; McCusker, L.B. Ionothermal synthesis and structure analysis of an open-framework zirconium phosphate with a high CO₂/CH₄ adsorption ratio. *Angew. Chem. Int. Ed.* **2011**, *50*, 8139–8142. [[CrossRef](#)]
163. Nakayama, M.; Sugiura, Y.; Hayakawa, T.; Nogami, M. A novel proton conductor of imidazole–aluminium phosphate hybrids in the solid state. *Phys. Chem. Chem. Phys.* **2011**, *13*, 9439–9444. [[CrossRef](#)]
164. Wang, K.; Li, T.; Zeng, H.; Zou, G.; Zhang, Q.; Zhien Lin, Z. Ionothermal synthesis of open-framework metal phosphates using a multifunctional ionic liquid. *Inorg. Chem.* **2018**, *57*, 8726–8729. [[CrossRef](#)]
165. Zhang, C.; Yan, Y.; Huang, Z.; Shi, H.; Zhang, C.; Cao, X.; Jiang, J. Triclinic AlPO₄-34 zeolite synthesized with nicotine and its proton conduction properties. *Inorg. Chem. Commun.* **2018**, *96*, 165–169. [[CrossRef](#)]
166. Xue, C.; Zou, Y.; Liu, S.-X.; Ren, X.-M.; Tian, Z.-F. Two different types of channels exhibiting distinct proton transport behaviour in an open framework aluminophosphate. *J. Solid State Chem.* **2018**, *258*, 695–701. [[CrossRef](#)]
167. Mu, Y.; Wang, Y.Y.; Li, Y.; Li, J.Y.; Yu, J.H. Organotemplate-free synthesis of an open-framework magnesium aluminophosphate with proton conduction properties. *Chem. Commun.* **2015**, *51*, 2149–2151. [[CrossRef](#)]
168. Fan, D.; Barrier, N.; Vicente, A.; Gilson, J.-P.; Clevers, S.; Dupray, V.; Coquereld, G.; Valtchev, V. Organic template-free synthesis of an open framework silicoaluminophosphate (SAPO) with high thermal stability and high ionic conductivity. *Inorg. Chem. Front.* **2020**, *7*, 542–553. [[CrossRef](#)]
169. Zhou, D.; Chen, L.; Yu, J.H.; Li, Y.; Yan, W.F.; Deng, F.; Xu, R.R. Synthesis, crystal structure, and solid-state NMR Spectroscopy of a new open-framework aluminophosphate (NH₄)₂Al₄(PO₄)₄(HPO₄)·H₂O. *Inorg. Chem.* **2005**, *44*, 4391–4397. [[CrossRef](#)] [[PubMed](#)]
170. Zhao, H.R.; Jia, Y.; Gu, V.; He, F.Y.; Zhang, K.M.; Tian, Z.F.; Liu, J.L. A 3D open-framework iron hydrogenophosphate showing high proton conductance under water and aqua-ammonia vapor. *RSC Adv.* **2020**, *10*, 9046–9051. [[CrossRef](#)]
171. Zima, V.; Lii, K.-H. Synthesis and characterization of a novel one-dimensional iron phosphate: $[\text{C}_4\text{H}_{12}\text{N}_2]_{1.5}[\text{Fe}_2(\text{OH})(\text{H}_2\text{PO}_4)(\text{HPO}_4)_2(\text{PO}_4)]$. *J. Chem. Soc. Dalton Trans.* **1998**, *24*, 4109–4112. [[CrossRef](#)]
172. Lii, K.-H.; Huang, Y.-F. Large tunnels in the hydrothermally synthesized open-framework iron phosphate (NH₃(CH₂)₃NH₃)₂[Fe₄(OH)₃(HPO₄)₃(PO₄)₃]. *Chem. Commun.* **1997**, *9*, 839–840. [[CrossRef](#)]
173. Bazaga-García, M.; Colodrero, R.M.P.; Papadaki, M.; Garczarek, P.; Zon, J.; Olivera-Pastor, P.; Losilla, E.R.; Reina, L.L.; Aranda, M.A.; Choquesillo-Lazarte, D.; et al. Guest Molecule-Responsive Functional Calcium Phosphonate Frameworks for Tuned Proton Conductivity. *J. Am. Chem. Soc.* **2014**, *136*, 5731–5739. [[CrossRef](#)]

174. Lim, D.-W.; Kitagawa, H. Proton Transport in Metal–Organic Frameworks. *Chem. Rev.* **2020**, *120*, 8416–8467. [[CrossRef](#)]
175. Mamlouk, M.; Scott, K. A boron phosphate-phosphoric acid composite membrane for medium temperature proton exchange membrane fuel cells. *J. Power Sources* **2015**, *286*, 290–298. [[CrossRef](#)]
176. Pusztai, P.; Haspel, H.; Tóth, I.Y.; Tombác, E.; László, K.; Kukovecz, Á.; Kónya, Z. Structure-Independent Proton Transport in Cerium(III) Phosphate Nanowires. *ACS Appl. Mater. Interfaces* **2015**, *7*, 9947–9956. [[CrossRef](#)] [[PubMed](#)]
177. Petersen, H.; Steffmann, N.; Fischer, M.; Zibrowius, I.R.; Philippi, W.; Schmidt, W.; Weidenthaler, C. Crystal structures of two titanium phosphate-based proton conductors: Ab initio structure solution and materials properties. *Inorg. Chem.* **2022**, *61*, 2379–2390. [[CrossRef](#)] [[PubMed](#)]